Stochastic Environmental Research and Risk Assessment (2023) 37:527–556
https://doi.org/10.1007/s00477-022-02267-2

ORIGINAL PAPER

Flood vulnerability of a few areas in the foothills of the Western Ghats: a comparison of AHP and F-AHP models

Chandini P. C. Senan[1] · R. S. Ajin[1,2] · Jean Homian Danumah[3] · Romulus Costache[4,5,6] · Alireza Arabameri[7] · A. Rajaneesh[8] · K. S. Sajinkumar[8,9] · Sekhar L. Kuriakose[1,10]

Accepted: 14 June 2022 / Published online: 20 July 2022

Abstract

Flooding is one of the most destructive natural catastrophes that can strike anywhere in the world. With the recent, but frequent catastrophic flood events that occurred in the narrow stretch of land in southern India, sandwiched between the Western Ghats and the Arabian Sea, this study was initiated. The goal of this research is to identify flood-vulnerable zones in this area by making the local self governing bodies as the mapping unit. This study also assessed the predictive accuracy of analytical hierarchy process (AHP) and fuzzy-analytical hierarchy process (F-AHP) models. A total of 20 indicators (nine physical-environmental variables and 11 socio-economic variables) have been considered for the vulnerability modelling. Flood-vulnerability maps, created using remotely sensed satellite data and geographic information systems, was divided into five zones. AHP and F-AHP flood vulnerability models identified 12.29% and 11.81% of the area as very high-vulnerable zones, respectively. The receiver operating characteristic (ROC) curve is used to validate these flood vulnerability maps. The flood vulnerable maps, created using the AHP and F-AHP methods, were found to be outstanding based on the area under the ROC curve (AUC) values. This demonstrates the effectiveness of these two models. The results of AUC for the AHP and F-AHP models were 0.946 and 0.943, respectively, articulating that the AHP model is more efficient than its chosen counterpart in demarcating the flood vulnerable zones. Decision-makers and land-use planners will find the generated vulnerable zone maps useful, particularly in implementing flood mitigation plans.

Keywords Flooding · Kerala · Physico-environmental vulnerability · Socio-economic vulnerability · Western Ghats

✉ R. S. Ajin
ajinares@ieee.org; ajinares@gmail.com

[1] Kerala State Emergency Operations Centre (KSEOC), Kerala State Disaster Management Authority (KSDMA), Thiruvananthapuram, India

[2] Resilience Development Initiative (RDI), Bandung, Indonesia

[3] Centre Universitaire de Recherche Et d'Application en Télédétection (CURAT), Université Félix Houphouët-Boigny, Abidjan, Côte d'Ivoire

[4] National Institute of Hydrology and Water Management, Bucharest, Romania

[5] Department of Civil Engineering, Transilvania University of Brasov, Brasov, Romania

[6] Danube Delta National Institute for Research and Development, Tulcea, Romania

[7] Department of Geomorphology, Tarbiat Modares University, Tehran, Iran

[8] Department of Geology, University of Kerala, Thiruvananthapuram, India

[9] Department of Geological and Mining Engineering and Sciences, Michigan Technological University, Houghton, Michigan, USA

[10] Centre for Disaster Resilience (CDR), Faculty for Geo-Information Science and Earth Observation (ITC), University of Twente, Enschede, The Netherlands

1 Introduction

Floods are one of the deadliest natural catastrophes occurring worldwide due to prolonged rainfall, but are aggravated by land-use changes, unscientific modifications of drainage channels, and unplanned development activities on flood plains and flood-prone areas (Deepak et al. 2020; Tehrany et al. 2015). Flood losses are generally categorized as direct or indirect as classified by Smith and Ward 1998. Direct losses are caused by physical contact of floodwater with individuals, property, or other items; whereas, indirect losses affect networks and social activities, resulting in losses such as traffic, trade, and public service interruptions (Nicholls et al. 2015), infectious disease outbreaks (Chadsuthi et al. 2021; Okaka and Odhiambo 2018), contamination of water resources (Ching et al. 2015; Sun et al. 2016; Yard et al. 2014), increased snakebite incidences (Ochoa et al. 2020), and psychological trauma (Crabtree 2013; Hajat et al. 2005; Paranjothy et al. 2011; Seyedin et al. 2017). Futhermore, delays and diverts in transportation networks cost money and loss of access to markets, affects employment prospects, health and education and social activities in far-flung places, which means that indirect losses are also incurred (Winter et al. 2016).

According to the Global Natural Disaster Assessment Report (2020), flood disasters with a frequency of 61.66% account for 40.92% of deaths, with 33.56% of the population affected, and 29.72% of direct economic losses worldwide for the year 2020. Out of the top ten countries, in terms of the number of people affected by flood disasters from 1900 to 2022, eight are from Asia (https://www.emdat.be/). Furthermore, in terms of the number of flood occurrences, out of the top ten countries (with 1,800 occurrences), seven countries are from Asia, which accounts for 1,339 occurrences (74.38%) (https://www.emdat.be/). The number of fatalities due to flooding are increasing in Asia (Franzke and Torelló i Sentelles 2020). Global warming and associated polar ice meltdown, glacier meltdown and sea-level rise are the major reasons for frequent flooding (Kumcu 2022; Swain et al. 2020a; Tabari 2020). Alike the rest of the world, flooding is one of the most prevalent natural hazards in India. India is one of the top ten countries (ranks third) most frequently affected by flooding (Liu et al. 2022). But what makes it different from the rest is the very high population density. According to EM-DAT (https://www.emdat.be/), the second highest number of deaths (30,115) was recorded in India after China due to riverine flooding between 1990 and 2022. In terms of total estimated damage during this time period, India ranks third (55.78 billion USD) after China and the United States (https://www.emdat.be/). Also, the total number of people affected by floods in India in the aforementioned period is 348,902,349, with China being at the top of the list (https://www.emdat.be/).

One of the recent catastrophic flood-affected areas in India is the narrow stretch of land, called Kerala, located between the Western Ghats and the Arabian Sea. Kerala is one of thestates in India having the highest population density (860 per km^2), and is nestled in the foothills of the Western Ghats, an orographic edifice. This state has 44 medium-to-small rivers, all with a short traverse of an average of 100–150 km, flowing through all the physiographic zones, viz., lowland, midland, and highland, before debouching into the Arabian Sea (Sajinkumar et al. 2022). Because of the preponderance of the monsoonal climate, many parts of Kerala have been severely battered by floods, with the recent floods being more devastating (i.e., the 2018, 2019, 2020, and 2021 floods). The severe floods of 2018 and 2019 caused significant damage to infrastructure and property, and resulted in hundreds of deaths in Kerala (Hao et al. 2020, 2022; Hunt and Menon 2020; Mishra and Shah 2018; Vanama et al. 2021; Vishnu et al. 2019, 2020). What makes more difficult to estimate the accurate losses are: (i) the lack of a clear strategy, (ii) absence of a single, reliable method for estimating damage and costs, (iii) non-availability of multiple, but diversified, agencies in post-disaster reconstruction activities, and (iv) the longer resilience time (Donnini et al. 2017).

One of the pressing requirements in studying the flooding events is the assessment of vulnerability. Researchers generally uses AHP (Dandapat and Panda 2017; Deepak et al. 2020; Desalegn and Mulu 2020; Hoque et al. 2019; Hussain et al. 2021; Radmehr and Araghinejad 2015), analytical network process (Chukwuma et al. 2021), Bayesian belief network (Abebe et al. 2018), Weight of evidence-information value (Saha et al. 2021), frequency ratio (FR) (Saha et al. 2021; Sarkar and Mondal 2020), F-AHP (Duan et al. 2021), and support vector machine (Duan et al. 2021) for assessing flood vulnerability. Feloni et al. (2020) created flood vulnerability maps of the Attica region in Greece using the AHP and fuzzy-analytical hierarchy process (F-AHP) methods. They used physical vulnerability indicating factors such as digital elevation model (DEM), slope, critical aspect, horizontal overland flow distance, vertical distance of channel network, curvature index, SAGA wetness index, composite curve number, and daily-modified Fournier index. Ali et al. (2019) compared FR and AHP for demarcating the flood vulnerable zones in the Sundarbans region of India. They used only the physical vulnerability factors such as slope, elevation, topographic wetness index, land use land cover, amount of rainfall deviation, distance from river, and clay content in soil. Also, no researchers compared the AHP and F-AHP models to identify flood vulnerable zones using both physical-environmental and socio-economic

indicators in any flood-prone area in the world. The majority of the existing literature focused solely on the areas' physical vulnerability factors (Desalegn and Mulu 2020; Feloni et al. 2020).

In any disaster study, the geographical ambience where the influencing parameters can be thoroughly studied could be a natural boundary like a drainage basin, whereas the implementation of management practices will be feasible within a political boundary. In India, the political set-up in the lowest rug is the local self governing (LSG) bodies. One of the worst-affected districts (which consist of a cluster of LSGs) is Kottayam (Vanama et al. 2021), located in the foothills of the Western Ghats, where the rivers Muvattupuzha, Meenachil, and Manimala were flooded during the recent years. Thus, this study aims to identify the flood vulnerable LSGs in the Kottayam district using both the AHP and F-AHP models, select the best one among these two models, and suggest suitable recommendations.

2 Materials and methods

2.1 Study area

Located beneath the Western Ghats, Kottayam district has longitudes of 76̊20′0' 'E and 77̊00′0'' E and latitudes of 9̊20′0'' N and 9̊55′0'' N and covers an area of about 2208 km^2 (Fig. 1). Kottayam district experiences a tropical climate, with an average annual rainfall of 3130.33 mm (https://kottayam.nic.in/climate/). The eastern part of the district is composed of Precambrian metamorphic rocks that form steep terrain; the central part is a low plateau with Tertiary sediments and laterites; and the western part is a low plain covered by Quaternary fluvial or partly marine formations (Department of Mining and Geology 2016). Meenachil, Muvattupuzha, and Manimala are the district's major rivers (https://kottayam.nic.in/en/geography/), all originating from the Western Ghats and debouching into the Vembanad Lake. The Meenachil River has a length of 78 km, whereas the Muvattupuzha and Manimala rivers have lengths of 121 and 92 km, respectively. According to the data acquired from the National Remote Sensing Centre, 185.82 km^2, 106.44 km^2, and 88.96 km^2 areas of the district were inundated by the floods that happened in the years 2018, 2019, and 2020, respectively. A total of 23 human fatalities have been recorded in Kottayam district during the 2018 monsoon season, while there were two during the 2019 monsoon season (Government of Kerala 2018a, 2018b, 2019a, b).

2.2 Data used

The modelling process involved the following five steps:

i. Data for the 20 vulnerability indicators were gathered from various sources (Table 1). The thematic layers of these vulnerability indicators were created using ArcGIS 10.8 and ERDAS Imagine 9.2.
ii. After creating the thematic layers of these indicators, the flood inundation data was gathered from the National Remote Sensing Centre (NRSC), India.
iii. Validation locations were randomly selected within the flood-inundated areas.
iv. The physical-environmental, socio-economic, and flood vulnerability maps were created using AHP and F-AHP methods. MS Excel and FisPro 3.8 were used to derive the weights of the AHP and F-AHP methods, respectively (Fig. 2).
v. The vulnerability maps were validated utilizing the receiver operating characteristic (ROC) curve method. Validation of the results was done using IBM SPSS 26.0 .

2.3 Methodology for vulnerability indicators

A total of 20 vulnerability indicators (nine physical-environmental variables and 11 socio-economic variables) have been considered. Physical-environmental vulnerability indicators such as slope angle, geomorphology, stream density, soil texture, land use/land cover (LULC), modified normalized difference water index (MNDWI), normalized difference vegetation index (NDVI), normalized difference built-up index (NDBI), water ratio index (WRI), and socio-economic vulnerability indicators such as total population, number of households, literacy rate, building roof type, building condition, household size, child population, access to information, building wall type, and marginalized populations (scheduled caste and scheduled tribe) have been utilized for the modelling.

2.3.1 Physical-environmental vulnerability indicators

Slope angle was computed from the ASTER GDEM using ArcGIS spatial (surface) analyst tools. The soil types of the study area were derived from the soil map published by the National Bureau of Soil Survey and Land Use Planning (NBSS&LUP) using ArcGIS tools. Land use and land cover (LULC) types of this area were derived from the Landsat 8 satellite images. The supervised maximum likelihood (cf. Joshi et al. 2022; Sisodia et al. 2014; Sunar Erbek et al. 2004) classification approach in the ERDAS Imagine software was utilized to classify the LULC types.

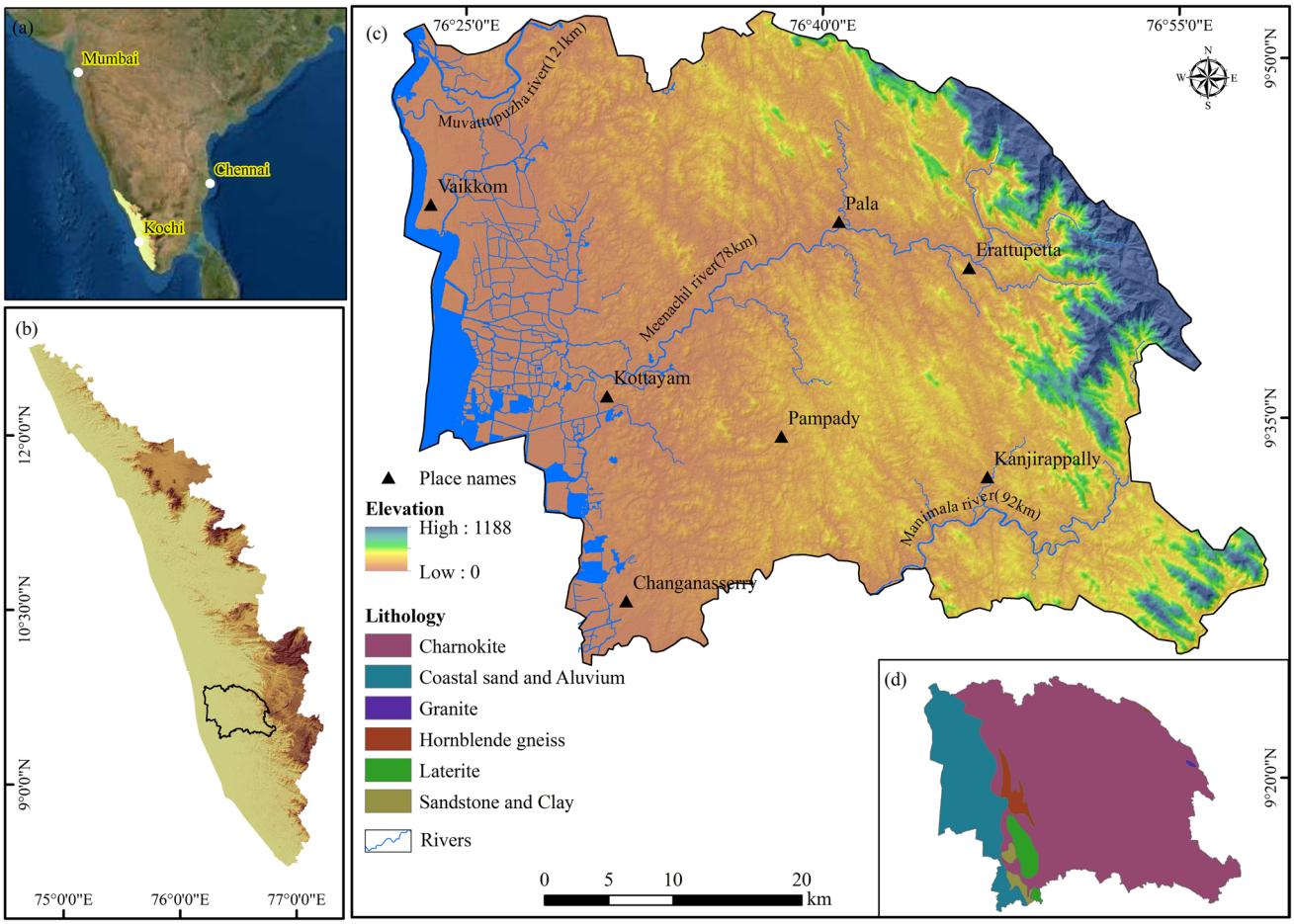

Fig. 1 Location map of the study area: **a**. South India, **b**. Kerala, **c**. elevation map with major rivers of the study area (Kottayam district), and **d**. Lithology map of the study area (Source: Elevation data of ASTER; Lithology data of Geological Survey of India)

Stream density was computed from the Survey of India (SoI) topographic map using ArcGIS spatial analyst (line density) tools. The geomorphic classes were initially derived from the Landsat 8 images through visual interpretation, but aided by field experience. This was verified with the SoI topographic map and high-resolution Google Earth images. This was done using ERDAS Imagine software. Water ratio index (WRI) was calculated using Eq. 1 (Shen and Li 2010) whereas modified normalized difference water index (MNDWI) was calculated using Eq. 2 (Xu 2006). Normalized difference built-up index (NDBI) was calculated using Eq. 3 (Zha et al. 2003) and normalized difference vegetation index (NDVI) was computed using Eq. 4 (Rouse et al. 1974).

The spectral indices such as WRI, MNDWI, NDBI, and NDVI were computed from the Landsat 8 images using ArcGIS spatial analyst (raster calculator) tool. The continuous data layers such as slope angle, stream density, WRI, MNDWI, NDBI, and NDVI were classified using the natural breaks method (cf. Ahmed 2015; Pradeep et al. 2022).

$$\mathrm{WRI} = \frac{(\mathrm{Green} + \mathrm{Red})}{(\mathrm{NIR} + \mathrm{MIR})} \tag{1}$$

where green, red, NIR and MIR stand for spectral reflectance of water in green, red, near-infrared and mid-infrared bands, respectively.

$$\mathrm{MNDWI} = \frac{(\mathrm{Green} - \mathrm{SWIR})}{(\mathrm{Green} + \mathrm{SWIR})} \tag{2}$$

where green, and SWIR stand for spectral reflectance of water in green, and short-wave infrared bands, respectively.

$$\mathrm{NDBI} = \frac{(\mathrm{SWIR1} - \mathrm{NIR})}{(\mathrm{SWIR1} + \mathrm{NIR})} \tag{3}$$

where SWIR, and NIR stand for spectral reflectance in short-wave infrared and near-infrared bands, respectively.

$$\mathrm{NDVI} = \frac{(\mathrm{NIR} - \mathrm{R})}{(\mathrm{NIR} + \mathrm{R})} \tag{4}$$

Table 1 Inventory on the data used in this study

Data	Source	Thematic layers derived	Scale/spatial resolution	Type of data
Topographic map	Survey of India	Stream density	1:50,000	Spatial
ASTER GDEM	https://earthexplorer.usgs.gov/	Slope	30 m	Spatial
Landsat 8 OLI image	https://earthexplorer.usgs.gov/	Land use/land cover, Geomorphology NDVI, MNDWI, NDBI WRI	30 m	Spatial
Soil map	National bureau of soil survey & Land use planning (NBSS&LUP)	Soil texture	1:250,000	Spatial
Census data	https://censusindia.gov.in/	Total population Number of households, Literacy rate, Building roof type, Building condition, Household size, Child population, Marginalized population 1, Marginalized population 2, Access to information, Building wall type	–	Non-spatial
Flood inundated data	National Remote Sensing centre	Flood inundated areas for the years 2018, 2019, and 2020	30 m	Spatial

where NIR and R stand for spectral reflectance in the near-infrared and red bands, respectively.

2.3.2 Socio-economic vulnerability indicators

All the eleven socio-economic vulnerability indicators were derived from the 2011 census data and were categorized into five classes through the natural breaks method (cf. Wubalem 2021) using ArcGIS tools.

2.4 AHP modeling

The AHP method, developed by Thomas L. Saaty (Saaty 1980) is used to make difficult problems into a hierarchy and find the best answer for the goal (Qazi and Abushammala 2020). The creation of the matrix for pair-wise comparisons, the computation of the eigen vector, the weighting coefficient (Tables 2 and 3), and the consistency ratio (Tables 4 and 5) are the major procedures involved with the AHP modelling (Akshaya et al. 2021; Amrutha et al. 2022; Nikhil et al. 2021; Thomas et al. 2021).

Using Eqs. 5 and 6, the eigen vector (Vp), and the weighting coefficient (Cp) were determined (as in Akshaya et al. 2021; Nikhil et al. 2021; Thomas et al. 2021).

$$V_P = \sqrt[k]{W1\mathrm{x}\ldots Wk} \tag{5}$$

where k = number of factors, and W = ratings.

$$C_p = \frac{Vp}{Vp1 + \ldots Vpk} \tag{6}$$

The priority vector [C], overall priority [D], and rational priority [E] were computed as in Danumah et al. (2016).

Equations 7, 8, and 9 (Akshaya et al. 2021; Nikhil et al. 2021; Thomas et al. 2021), were employed to compute the eigen value (λmax), consistency index (CI), and consistency ratio (CR).

$$\lambda_{\max} = \frac{[E]}{k} \tag{7}$$

$$\mathrm{CI} = {}^{(\lambda_{\max} - k)}/_{(k-1)} \tag{8}$$

$$CR = \frac{CI}{RI} \tag{9}$$

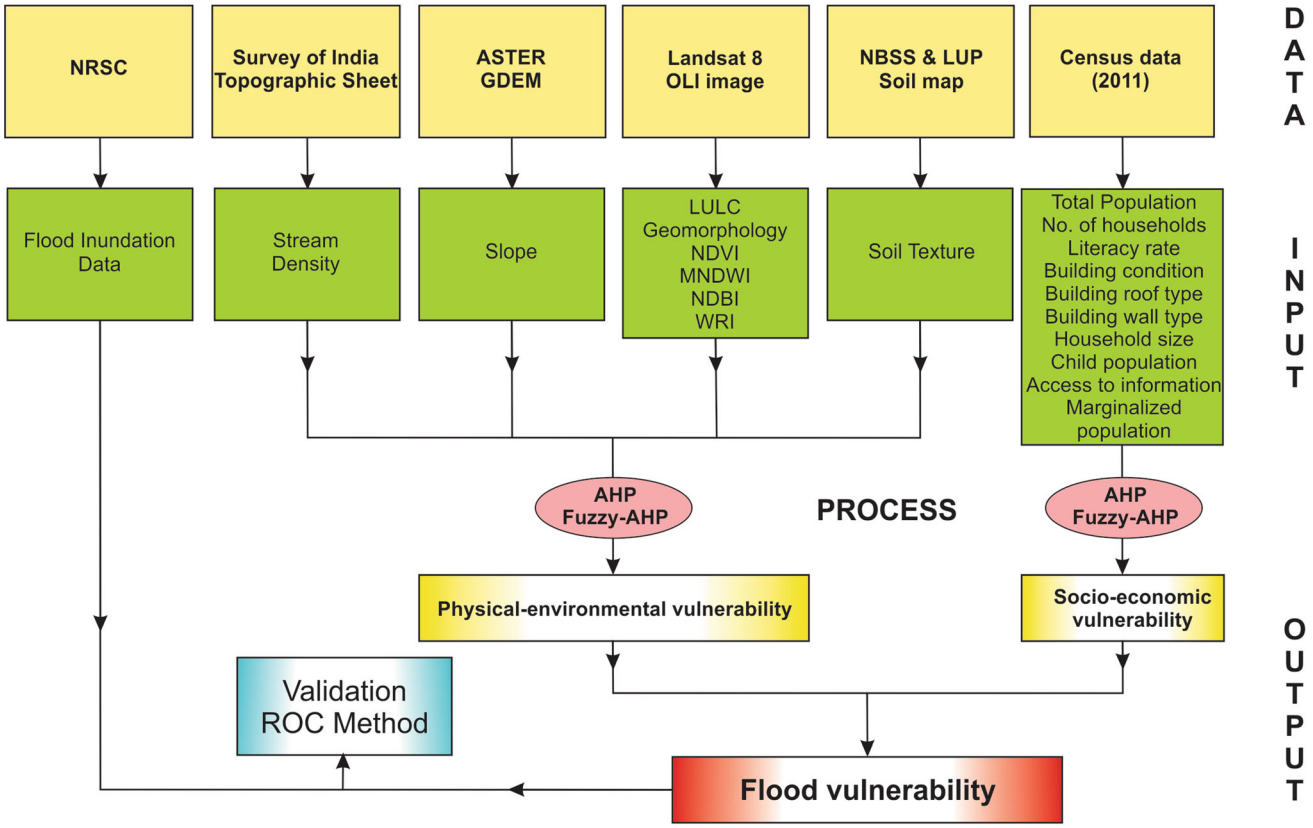

Fig. 2 Flowchart of the vulnerability modelling

Table 2 Pairwise comparison matrix for Physical-environmental indicators

	Slp.	Soil	LULC	SD	Geom.	WRI	MNDWI	NDBI	NDVI	Vp	Cp
Slp.	1	2	3	4	5	6	7	8	9	4.147	0.308
Soil	1/2	1	2	3	4	5	6	7	8	3.008	0.223
LULC	1/3	1/2	1	2	3	4	5	6	7	2.113	0.157
SD	1/4	1/3	1/2	1	2	3	4	5	6	1.459	0.108
Geom.	1/5	1/4	1/3	1/2	1	2	3	4	5	1.000	0.074
WRI	1/6	1/5	1/4	1/3	1/2	1	2	3	4	0.685	0.051
MNDWI	1/7	1/6	1/5	1/4	1/3	1/2	1	2	3	0.473	0.035
NDBI	1/8	1/7	1/6	1/5	1/4	1/3	1/2	1	2	0.332	0.025
NDVI	1/9	1/8	1/7	1/6	1/5	1/4	1/3	1/2	1	0.241	0.018
$\sum$	2.83	4.72	7.59	11.45	16.28	22.08	28.83	36.50	45.00	13.46	1.00

*Where Slp. is the slope, SD is the stream density, and Geom. is the geomorphology

where RI = random index (Saaty 1980).

Saaty (1980) considers a CR of less than 0.1 acceptable. If the CR is larger than 0.1, repeat the analysis until the CR is acceptable. The CR (0.031) in this AHP modelling is found acceptable. As a result, the outcomes are reliable.

The weights derived by the AHP model for the physical-environmental vulnerability (PEV) and socio-economic vulnerability (SEV) indicators are depicted in Eqs. 10 and 11.

$$\begin{aligned} \text{PEV} &= (0.308 \times \text{Slp.}) + (0.223 \times \text{Soil}) + (0.157 \times \text{LULC}) \\ &\quad + (0.108 \times \text{SD}) + (0.074 \times \text{Geom.}) \\ &\quad + (0.051 \times \text{WRI}) + (0.035 \times \text{MNDWI}) \\ &\quad + (0.025 \times \text{NDBI}) + (0.018 \times \text{NDVI}) \end{aligned} \tag{10}$$

Table 3 Pairwise comparison matrix for socio-economic vulnerability

	TP	NH	LR	BRT	BC	HHS	CP	MP1	MP2	ATI	BWT	Vp	Cp
TP	1	2	3	4	5	6	7	8	9	10	11	3.202	0.187
NH	1/2	1	2	3	4	5	6	7	8	9	10	2.462	0.144
LR	1/3	½	1	2	3	4	5	6	7	8	9	1.848	0.108
BRT	1/4	1/3	1/2	1	2	3	4	5	6	7	8	1.413	0.082
BC	1/5	¼	1/3	1/2	1	2	3	4	5	6	7	1.271	0.074
HHS	1/6	1/5	1/4	1/3	1/2	1	2	3	4	5	6	1.244	0.073
CP	1/7	1/6	1/5	1/4	1/3	1/2	1	2	3	4	5	1.221	0.071
MP1	1/8	1/7	1/6	1/5	1/4	1/3	1/2	1	2	3	4	1.194	0.070
MP2	1/9	1/8	1/7	1/6	1/5	1/4	1/3	1/2	1	2	3	1.158	0.067
ATI	1/10	1/9	1/8	1/7	1/6	1/5	1/4	1/3	1/2	1	2	1.105	0.064
BWT	1/11	1/10	1/9	1/8	1/7	1/6	1/5	1/4	1/3	1/2	1	1.038	0.060
$\sum$	3.02	4.93	7.83	11.72	16.59	22.45	29.28	37.08	45.83	55.50	66.00	17.16	1.00

*Where TP is the total population, NH is the number of households, LR is the literacy rate, BRT is the building roof types, BC is the building condition, HHS is the household size, CP is the child population, MP1 is the marginalized population 1 (SC), MP2 is the marginalized population 2 (ST), ATI is the access to information, and BWT is the building wall types

$$\begin{aligned} \text{SEV} = {} & (0.187 \times \text{TP}) + (0.144 \times \text{NH}) + (0.082 \times \text{BRT}) \\ & + (0.074 \times \text{BC}) + (0.073 \times \text{HHS}) + (0.071 \times \text{CP}) \\ & + (0.070 \times \text{MP1}) + (0.067 \times \text{MP2}) \\ & + (0.064 \times \text{ATI}) + (0.060 \times \text{BWT}) \end{aligned} \tag{11}$$

2.5 F-AHP modeling

A combination of AHP and fuzzy logic theory was employed to weight the relevant factors in the F-AHP model (Eskandari and Miesel 2017). The F-AHP model overcomes the limitations of the AHP model by allowing decision-makers to assess their preferences within an acceptable interval (Afolayan et al. 2020). Buckley (1985) presented a method for comparing fuzzy ratios that has been adopted for the study. The key procedures involved are pair-wise comparison matrix creation (see Tables 6 and 7), geometric mean calculation (see Tables 8 and 9), determination of relative fuzzy weights, and computation of averaged and normalized relative weights (see Tables 10 and 11). The following are the steps in F-AHP modelling:

Step 1 Comparison of the indicators or alternatives.

The fuzzy triangular scale (2, 3, 4) will be used when factor 1 (P1) is less significant than factor 2 (P2). For the comparison matrix, the fuzzy triangle scale will be (1/4, 1/3, 1/2) (Ayhan 2013).

Equation 12 depicts the matrix.

$$\tilde{A}^k = \begin{bmatrix} \tilde{d}^k_{11} & \tilde{d}^k_{12} & \ldots & \tilde{d}^k_{1n} \\ \tilde{d}^k_{21} & \ldots & \ldots & \tilde{d}^k_{2n} \\ \ldots & \ldots & \ldots & \ldots \\ \tilde{d}^k_{n1} & \tilde{d}^k_{n2} & \ldots & \tilde{d}^k_{mn} \end{bmatrix} \tag{12}$$

where $\tilde{d}^k_{ij}$ by way of fuzzy triangular numbers, reflects the kth decision maker's preference for the ith factor over the jth factor (Ayhan 2013).

Step 2 $\tilde{d}_{ij}$ was computed using Eq. 13, after averaging the preferences ($\tilde{d}^k_{ij}$)

$$\tilde{d}_{ij} = \frac{\sum_{k=1}^{K} \tilde{d}^k_{ij}}{K} \tag{13}$$

Step 3 The matrix was modified applying Eq. 14.

$$\tilde{A} = \begin{bmatrix} \tilde{d}_{11} & \cdots & \tilde{d}_{1n} \\ \vdots & \ddots & \vdots \\ \tilde{d}_{n1} & \cdots & \tilde{d}_{nn} \end{bmatrix} \tag{14}$$

Step 4 Computation of the geometric average using (Buckley 1985) Eq. 15

$$\tilde{r}_i = \left(\prod_{j=1}^{n} \tilde{d}_{ij} \right)^{1/n}, i = 1, 2, ..., n \tag{15}$$

where $\tilde{r}_i$ = triangular values.

Step 5 Computation of fuzzy weight using the following three sub processes (5a, 5b, and 5c).

5a: Computation of vector summation of each $\tilde{r}_i$

5b: The fuzzy triangular number was substituted to convert it to an increasing order, after determining the (-1) power of the summation vector.

5c: Computation of fuzzy weights: Each $\tilde{r}_i$ was multiplied with its reverse vector as in Eq. 16 to compute the weights

$$\begin{aligned} \tilde{w}_i = {} & \tilde{r}_i \otimes (\tilde{r}_1 \oplus \tilde{r}_2 \oplus \ldots \oplus \tilde{r}_n)^{-1} \\ = {} & (lw_i, mw_i, uw_i) \end{aligned} \tag{16}$$

Table 4 Normalized matrix for physical-environmental vulnerability

	Slp.	Soil	LULC	SD	Geom.	WRI	MNDWI	NDBI	NDVI	∑ rank	[C]	[D] = [A]*[C]	[E] = [D]/[C]	λmax	CI	CR
Slp.	0.35	0.42	0.40	0.35	0.31	0.27	0.24	0.22	0.20	2.76	0.307	2.981	9.711	9.408	0.051	0.035 (3.52%)
Soil	0.18	0.21	0.26	0.26	0.25	0.23	0.21	0.19	0.18	1.96	0.218	2.134	9.782			
LULC	0.12	0.11	0.13	0.17	0.18	0.18	0.17	0.16	0.16	1.39	0.154	1.499	9.715			
SD	0.09	0.07	0.07	0.09	0.12	0.14	0.14	0.14	0.13	0.98	0.109	1.040	9.548			
Geom.	0.07	0.05	0.04	0.04	0.06	0.09	0.10	0.11	0.11	0.69	0.076	0.714	9.345			
WRI	0.06	0.04	0.03	0.03	0.03	0.05	0.07	0.08	0.09	0.48	0.053	0.489	9.168			
MNDWI	0.05	0.04	0.03	0.02	0.02	0.02	0.03	0.05	0.07	0.33	0.037	0.336	9.077			
NDBI	0.04	0.03	0.02	0.02	0.02	0.02	0.02	0.03	0.04	0.23	0.026	0.236	9.104			
NDVI	0.04	0.03	0.02	0.01	0.01	0.01	0.01	0.01	0.02	0.17	0.019	0.174	9.222			
∑	1.00	1.00	1.00	1.00	1.00	1.00	1.00	1.00	1.00	9.00	1.000		84.672			

Table 5 Normalized matrix for socio-economic vulnerability

	TP	NH	LR	BRT	BC	HHS	CP	MP1	MP2	ATI	BWT	∑ rank	[C]	[D] = [A]*[C]	[E] = [D]/[C]	λ_{max}	CI	CR
TP	0.33	0.41	0.38	0.34	0.30	0.27	0.24	0.22	0.20	0.18	0.17	3.03	0.275	3.368	12.236	11.648	0.065	0.045
NH	0.17	0.20	0.26	0.26	0.24	0.22	0.20	0.19	0.17	0.16	0.15	2.23	0.202	2.506	12.386			(4.47%)
LR	0.11	0.10	0.13	0.17	0.18	0.18	0.17	0.16	0.15	0.14	0.14	1.63	0.149	1.737	11.689			
BRT	0.08	0.07	0.06	0.09	0.12	0.13	0.14	0.13	0.13	0.13	0.12	1.20	0.109	1.332	12.173			
BC	0.07	0.05	0.04	0.04	0.06	0.09	0.10	0.11	0.11	0.11	0.11	0.89	0.080	0.957	11.897			
HHS	0.06	0.04	0.03	0.03	0.03	0.04	0.07	0.08	0.09	0.09	0.09	0.65	0.059	0.683	11.594			
CP	0.05	0.03	0.03	0.02	0.02	0.02	0.03	0.05	0.07	0.07	0.08	0.47	0.043	0.486	11.324			
MP1	0.04	0.03	0.02	0.02	0.02	0.01	0.02	0.03	0.04	0.05	0.06	0.34	0.031	0.345	11.143			
MP2	0.04	0.03	0.02	0.01	0.01	0.01	0.01	0.01	0.02	0.04	0.05	0.25	0.022	0.248	11.096			
ATI	0.03	0.02	0.02	0.01	0.01	0.01	0.01	0.01	0.01	0.02	0.03	0.18	0.016	0.183	11.198			
BWT	0.03	0.02	0.01	0.01	0.01	0.01	0.01	0.01	0.01	0.01	0.02	0.14	0.012	0.141	11.388			
∑	1.00	1.00	1.00	1.00	1.00	1.00	1.00	1.00	1.00	1.00	1.00	11.00	1.000		128.124			

Table 6 Pair-wise comparisons of factors of physical-environmental vulnerability

	Slp.			Soil			LULC			SD			Geom.			WRI			MNDWI			NDBI			NDVI		
Slp.	1	1	1	1	2	3	2	3	4	3	4	5	4	5	6	5	6	7	6	7	8	7	8	9	9	9	9
Soil	1/3	1/2	1	1	1	1	1	2	3	2	3	4	3	4	5	4	5	6	5	6	7	6	7	8	7	8	9
LULC	1/4	1/3	1/2	1/3	1/2	1	1	1	1	1	2	3	2	3	4	3	4	5	4	5	6	5	6	7	6	7	8
SD	1/5	1/4	1/3	1/4	1/3	1/2	1/3	1/2	1	1	1	1	1	2	3	2	3	4	3	4	5	4	5	6	5	6	7
Geom.	1/6	1/5	1/4	1/5	1/4	1/3	1/4	1/3	1/2	1/3	1/2	1	1	1	1	1	2	3	2	3	4	3	4	5	4	5	6
WRI	1/7	1/6	1/5	1/6	1/5	1/4	1/5	1/4	1/3	1/4	1/3	1/2	1/3	1/2	1	1	1	1	1	2	3	2	3	4	3	4	5
MNDWI	1/8	1/7	1/6	1/7	1/6	1/5	1/6	1/5	1/4	1/5	1/4	1/3	1/4	1/3	1/2	1/3	1/2	1	1	1	1	1	2	3	2	3	4
NDBI	1/9	1/8	1/7	1/8	1/7	1/6	1/7	1/6	1/5	1/6	1/5	1/4	1/5	1/4	1/3	1/4	1/3	1/2	1/3	1/2	1	1	1	1	1	2	3
NDVI	1/9	1/9	1/9	1/9	1/8	1/7	1/8	1/7	1/6	1/7	1/6	1/5	1/6	1/5	1/4	1/5	1/4	1/3	1/4	1/3	1/2	1/3	1/2	1	1	1	1

Table 7 Pair-wise comparisons of factors of socio-economic vulnerability

	TP			NH			LR			BRT			BC			HHS			CP			MP1			MP2			ATI			BWT		
TP	1	1	1	1	2	3	2	3	4	3	4	5	4	5	6	5	6	7	6	7	8	7	8	9	8	9	10	9	10	11	11	11	11
NH	1/3	1/2	1	1	1	1	1	2	3	2	3	4	3	4	5	4	5	6	5	6	7	6	7	8	7	8	9	8	9	10	9	10	11
LR	1/4	1/3	1/2	1/3	1/2	1	1	1	1	1	2	3	2	3	4	3	4	5	4	5	6	5	6	7	6	7	8	7	8	9	8	9	10
BRT	1/5	1/4	1/3	1/4	1/3	1/2	1/3	1/2	1	1	1	1	1	2	3	2	3	4	3	4	5	4	5	6	5	6	7	6	7	8	7	8	9
BC	1/6	1/5	1/4	1/5	1/4	1/3	1/4	1/3	1/2	1/3	1/2	1	1	1	1	1	2	3	2	3	4	3	4	5	4	5	6	5	6	7	6	7	8
HHS	1/7	1/6	1/5	1/6	1/5	1/4	1/5	1/4	1/3	1/4	1/3	1/2	1/3	1/2	1	1	1	1	1	2	3	2	3	4	3	4	5	4	5	6	5	6	7
CP	1/8	1/7	1/6	1/7	1/6	1/5	1/6	1/5	1/4	1/5	1/4	1/3	1/4	1/3	1/2	1/3	1/2	1	1	1	1	1	2	3	2	3	4	3	4	5	4	5	6
MP1	1/9	1/8	1/7	1/8	1/7	1/6	1/7	1/6	1/5	1/6	1/5	1/4	1/5	1/4	1/3	1/4	1/3	1/2	1/3	1/2	1	1	1	1	1	2	3	2	3	4	3	4	5
MP2	1/10	1/9	1/8	1/9	1/8	1/7	1/8	1/7	1/6	1/7	1/6	1/5	1/6	1/5	1/4	1/5	1/4	1/3	1/4	1/3	1/2	1/3	1/2	1	1	1	1	1	2	3	2	3	4
ATI	1/11	1/10	1/9	1/10	1/9	1/8	1/9	1/8	1/7	1/8	1/7	1/6	1/7	1/6	1/5	1/6	1/5	1/4	1/5	1/4	1/3	1/4	1/3	1/2	1/3	1/2	1	1	1	1	1	2	3
BWT	1/11	1/11	1/11	1/11	1/10	1/9	1/10	1/9	1/8	1/9	1/8	1/7	1/8	1/7	1/6	1/7	1/6	1/5	1/6	1/5	1/4	1/5	1/4	1/3	1/4	1/3	1/2	1/3	1/2	1	1	1	1

Table 8 Geometric means of fuzzy comparison values: Physical-environmental vulnerability

	Fuzzy geometric mean value ($\bar{t}i$)		
Slp.	3.292	4.147	4.902
Soil	2.282	3.008	3.840
LULC	1.576	2.113	2.785
SD	1.080	1.459	1.956
Geom.	0.740	1.000	1.351
WRI	0.511	0.685	0.926
MNDWI	0.359	0.473	0.634
NDBI	0.260	0.332	0.438
NDVI	0.204	0.241	0.304
$\sum \bar{t}i$	10.305	13.460	17.136
$(\sum \bar{t}i)^{-1}$	0.058	0.074	0.097

Table 9 Geometric means of fuzzy comparison values: socio-economic vulnerability

	Fuzzy geometric mean value ($\bar{t}i$)		
TP	3.98	4.91	5.73
NH	2.90	3.71	4.61
LR	2.09	2.72	3.48
BRT	1.50	1.96	2.55
BC	1.07	1.40	1.84
HHS	0.76	1.00	1.32
CP	0.54	0.71	0.94
MP1	0.39	0.51	0.67
MP2	0.29	0.37	0.48
ATI	0.22	0.27	0.35
BWT	0.17	0.20	0.25
$\sum \bar{t}i$	13.903	17.768	22.221
$(\sum \bar{t}i)^{-1}$	0.045	0.056	0.072

Table 10 Relative fuzzy weights, averaged and normalized relative weights: Physical-environmental vulnerability

	Fuzzy weight			Weight (wi)	Normalized weight
	$[\bar{W}i = \bar{t}i * ((\Sigma \bar{t}i)^{-1})]$				
Slp.	0.192	0.308	0.476	0.325	0.299
Soil	0.133	0.223	0.373	0.243	0.223
LULC	0.092	0.157	0.270	0.173	0.159
SD	0.063	0.108	0.190	0.120	0.111
Geom.	0.043	0.074	0.131	0.083	0.076
WRI	0.030	0.051	0.090	0.057	0.052
MNDWI	0.021	0.035	0.062	0.039	0.036
NDBI	0.015	0.025	0.043	0.027	0.025
NDVI	0.012	0.018	0.029	0.020	0.018
$\sum$				1.09	1.00

Table 11 Relative fuzzy weights, averaged and normalized relative weights: Socio-economic vulnerability

	Fuzzy weight			Weight (wi)	Normalized weight
	$[\bar{W}i = \bar{t}i * ((\Sigma \bar{t}i)^{-1})]$				
TP	0.179	0.276	0.412	0.289	0.269
NH	0.130	0.209	0.332	0.224	0.208
LR	0.094	0.153	0.250	0.166	0.154
BRT	0.067	0.111	0.184	0.121	0.112
BC	0.048	0.079	0.133	0.087	0.081
HHS	0.034	0.056	0.095	0.062	0.057
CP	0.024	0.040	0.068	0.044	0.041
MP1	0.018	0.029	0.048	0.031	0.029
MP2	0.013	0.021	0.034	0.023	0.021
ATI	0.010	0.015	0.025	0.017	0.020
BWT	0.008	0.011	0.018	0.012	0.012
$\sum$				1.07	1.00

Step 6 Eq. 17 was utilized for the de-fuzzification of fuzzy weights (Chou and Chang 2008)

$$M_i = \frac{lw_i, mw_i, uw_i}{3} \tag{17}$$

Step 7 Standardization of Mi using Eq. 18.

$$N_i = \frac{M_i}{\sum_{i=1}^{n} M_i} \tag{18}$$

The weights derived by the F-AHP model for the PEV and SEV indicators are depicted in Eqs. 19 and 20.

$$\begin{aligned} \text{PEV} = &(0.299 \times \text{Slp.}) + (0.223 \times \text{Soil}) + (0.159 \times \text{LULC}) \\ &+ (0.111 \times \text{SD}) + (0.076 \times \text{Geom.}) + \\ &(0.052 \times \text{WRI}) + (0.036 \times \text{MNDWI}) \\ &+ (0.025 \times \text{NDBI}) + (0.018 \times \text{NDVI}) \end{aligned} \tag{19}$$

$$\begin{aligned} \text{SEV} = &(0.269 \times \text{TP}) + (0.208 \times \text{NH}) + (0.154 \times \text{LR}) \\ &+ (0.112 \times \text{BRT}) + (0.081 \times \text{BC}) + (0.057 \times \text{HHS}) \\ &+ (0.041 \times \text{CP}) + (0.029 \times \text{MP1}) + (0.021 \times \text{MP2}) \\ &+ (0.020 \times \text{ATI}) + (0.012 \times \text{BWT}) \end{aligned} \tag{20}$$

2.6 Validation of modelling results using the ROC method

ROC graphs are widely used to evaluate a classifier's performance. On the y-axis, sensitivity is plotted, while 1-specificity is plotted on the x-axis (Grimnes and Martinsen 2015). The AUC is a single scalar statistic that quantifies a binary classifier's total performance (Hanley and McNeil 1982). An AUC value of 0.7 to 0.8 is acceptable, 0.8 to 0.9 is excellent, and more than 0.9 is outstanding (Hosmer and Lemeshow 2000). The results of the study were validated using the flood inundation data provided by the NRSC for the years 2018, 2019, and 2020 (Fig. 3a, 3b, and 3c). In this research, a total of 100 locations within the flood-inundated areas have been randomly selected as a validation dataset (Fig. 4). The SPSS software was utilized for plotting the ROC graph and estimating the AUC values.

3 Results

3.1 Vulnerability indicators

3.1.1 Slope angle

When the slope angle is less, the probability of flooding increases (Rahman et al. 2019). Runoff from rainfall accumulates and inundates areas with gentle slopes due to the low flow velocity in these areas (Lee and Kim 2021). The slope of the district ranges from 0 to 74.48° (Fig. 5a) and is categorized into five zones (0–4.67°, 4.68–9.93°, 9.94–17.52°, 17.53–27.75°, and 27.76–74.48°). The western portion of the district has gentle slopes, while the northeastern portion has steeper slopes.

3.1.2 Soil texture

The greater the infiltration rate of soil, the less likely a flood will occur (Islam et al. 2021). Impermeable formations, such as clay, enhance runoff rates, increasing the

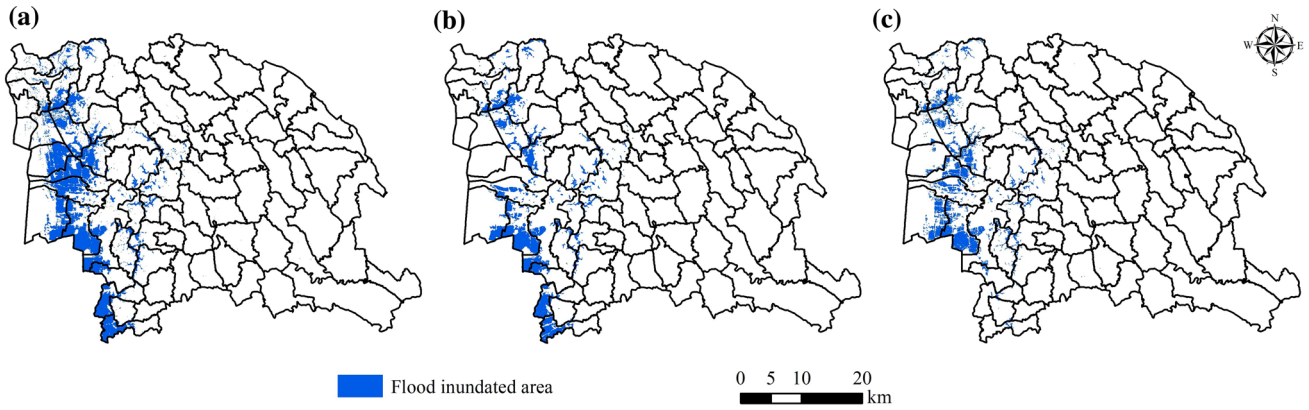

Fig. 3 **a**. 2018 Flood inundated area; **b**. 2019 Flood inundated area; **c**. 2020 Flood inundated area

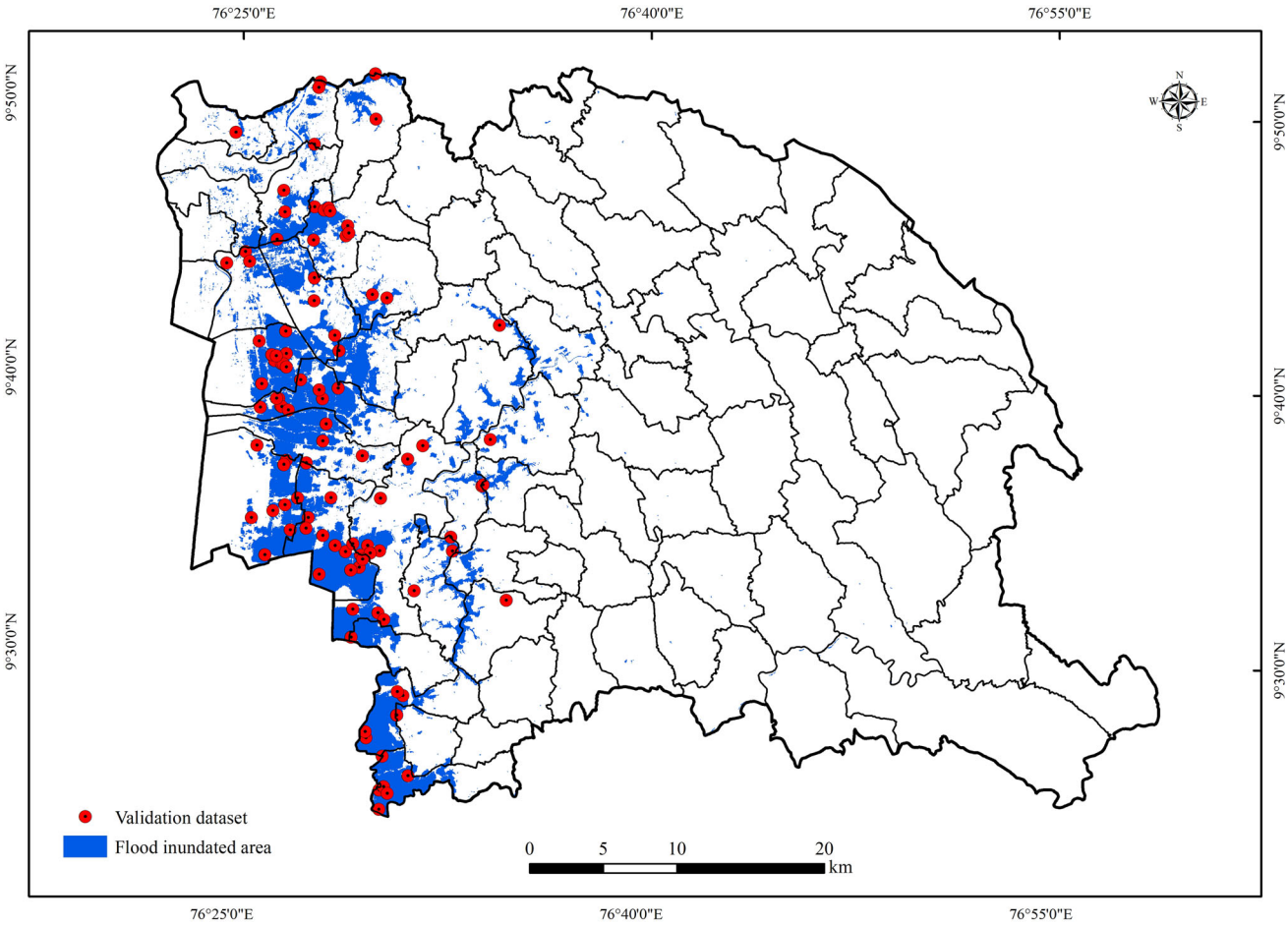

Fig. 4 Flood inundation data (2018–2020) and validation dataset

probability of flooding (Swain et al. 2020b). On the basis of soil texture, the soils are classified into clay, gravelly clay, gravelly loam, loam, and sand (Fig. 5b). The lower elevated parts of the district have predominantly clayey soil.

3.1.3 Land use/land cover (LULC)

Flooding is more likely in built-up areas because water cannot infiltrate and generate surface runoff (Islam et al. 2021). Increased forest and vegetation cover enhances

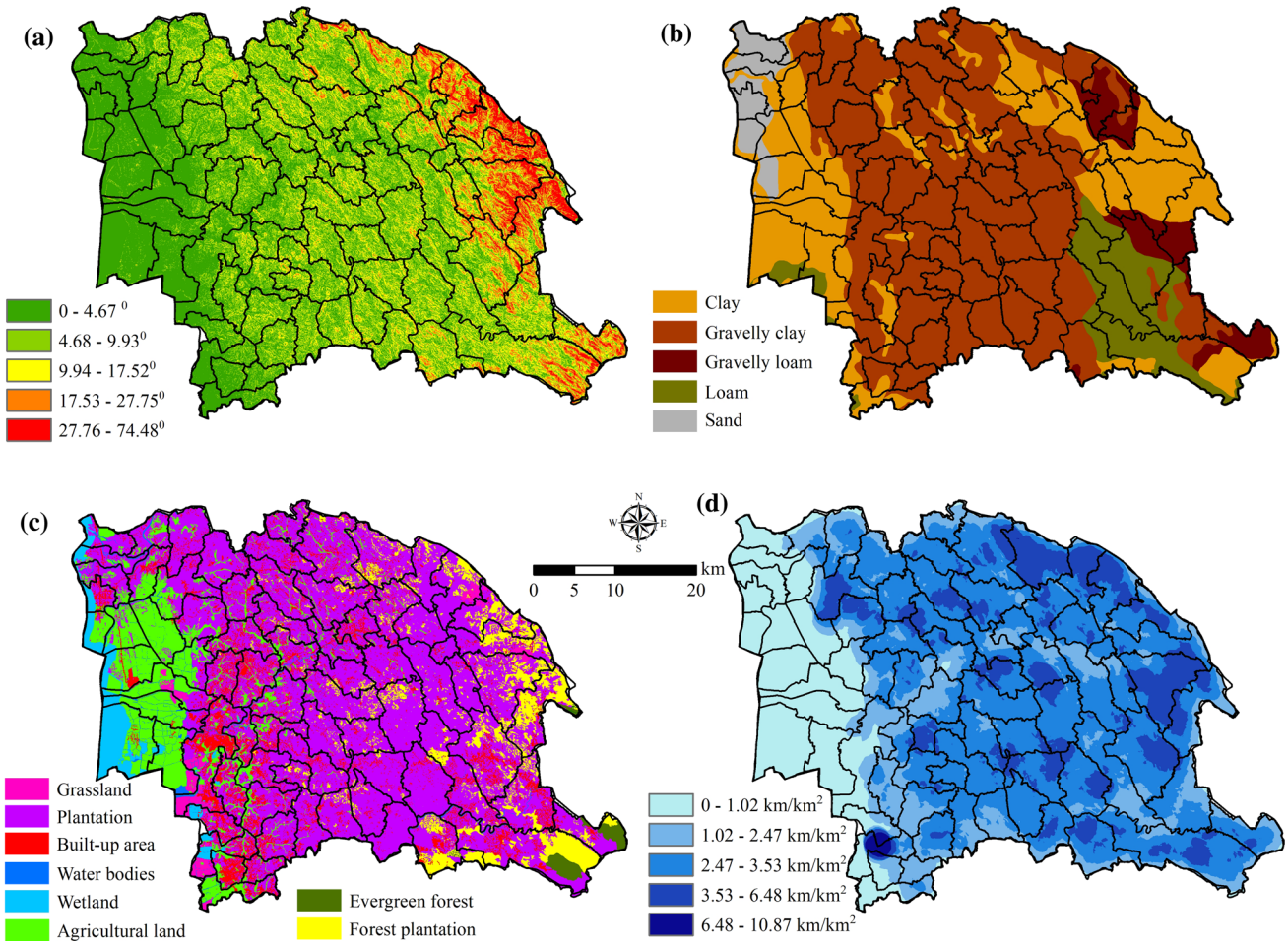

Fig. 5 **a**. Slope; **b**. Soil types; **c**. Land use/land cover types; **d**. Stream density

water infiltration and reduces runoff depth, thus lowering the chance of flooding (Swain et al. 2020b). The land use/land cover (LULC) types comprise agricultural land, forest plantations, grassland, plantations (mixed vegetation), evergreen forest, built-up areas, water bodies, and wetlands (Fig. 5c). Agricultural land (paddy fields) and wetlands dominate the low-elevation part of the study area.

3.1.4 Stream density

Flooding is more likely in locations with lower stream densities because there aren't enough streams to drain out the surplus rainwater (Ajin et al. 2013; 2019). On the basis of the density of stream channels, the district is categorized into five zones (0–1.02 km/km^2, 1.02–2.47 km/km^2, 2.47–3.53 km/km^2, 3.53–6.48 km/km^2, and 6.48–10.87 km/km^2). The lower elevation region of the study area has a stream density ranging from 0 to 1.02 km/sq.km (Fig. 5d).

3.1.5 Geomorphology

The geomorphic classes of the study area comprise the coastal plain, denudational hills, floodplain, islands, and plateau (Fig. 6a). The coastal plain and floodplains, located in the lower elevated region of the study area, are more susceptible to flooding due to flat topography, which favours inundation.

3.1.6 Water ratio index (WRI)

Shen and Li (2010) suggest a WRI with a value greater than 1 for waterbodies. WRI values less than or close to 1 (especially values closer to and below zero) indicate that the soil moisture content is higher, making the area more vulnerable to flooding. The WRI of Kottayam district ranges from 0.30 to 1.45 and is grouped into five zones (0.30–0.54, 0.55–0.62, 0.63–0.78, 0.79–1.09, and 1.10–1.45) as depicted in Fig. 6b. The low elevated regions have a WRI value above 1.

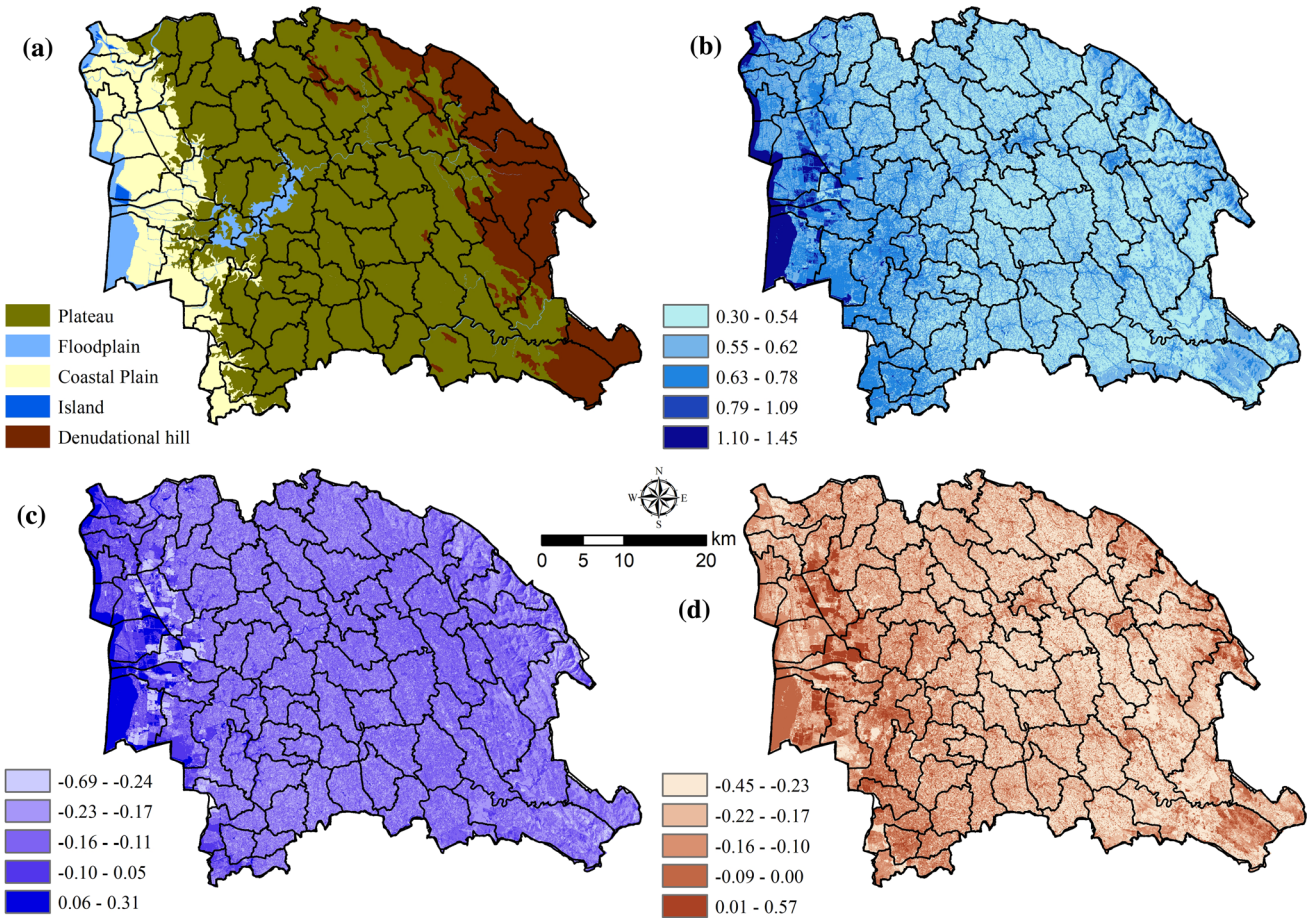

Fig. 6 **a**. Geomorphology; **b**. Water ratio index; **c**. Modified normalized difference water index; **d**. Normalized difference built-up index

3.1.7 Modified normalized difference water index (MNDWI)

The MNDWI (Xu 2006) suggests greater positive values for water bodies and smaller negative values for soil, vegetation, and built-up areas (Du et al. 2016). The higher MNDWI values represent areas with higher soil moisture content and are more vulnerable to flooding. The MNDWI of the study area ranges from -0.69 to 0.31 and is grouped into five zones (− 0.69 to − 0.24, − 0.23 to − 0.17, − 0.16 to − 0.11, − 0.10 to 0.05, and 0.06 to 0.31) as depicted in Fig. 6c. The low-elevated regions of the study area have positive MNDWI values and hence, more vulnerable to flooding.

3.1.8 Normalized difference built-up index (NDBI)

The positive NDBI values show built-up areas (Shahfahad et al. 2021). Urbanization increases the amount of impervious surface area in a location, slowing the hydrologic system's response time and thereby increasing the risk of flooding (Feng et al. 2021). The NDBI of the study area ranges from − 0.45 to 0.57 and is grouped into five zones (− 0.45 to − 0.23, − 0.22 to − 0.17, − 0.16 to − 0.10, − 0.09 to 0.00, and 0.01 to 0.57) as depicted in Fig. 6d. The low-elevated regions of the area have positive NDBI value and hence, induce flooding.

3.1.9 Normalized difference vegetation index (NDVI)

The NDVI ranges between − 1 and + 1 (Gessesse and Melesse 2019), and densely vegetated areas will be represented by positive values, and water and built-up areas, on the other hand, will be indicated by near-zero or negative values (Viana et al. 2019). The possibility of flooding is high in areas with lower NDVI values, as these values represent non-vegetated areas where the chance of surface runoff is greater. The thick vegetative cover can improve water infiltration and reduce runoff depth, lowering the risk of flooding (Swain et al. 2020b). The NDVI of the study area ranges from − 0.11 to 0.59 and is grouped into five zones (− 0.11 to 0.08, 0.09 to 0.25, 0.26 to 0.34, 0.35 to 0.41, and 0.42 to 0.59) as depicted in Fig. 7. The low-elevated regions of the study area have negative NDVI values.

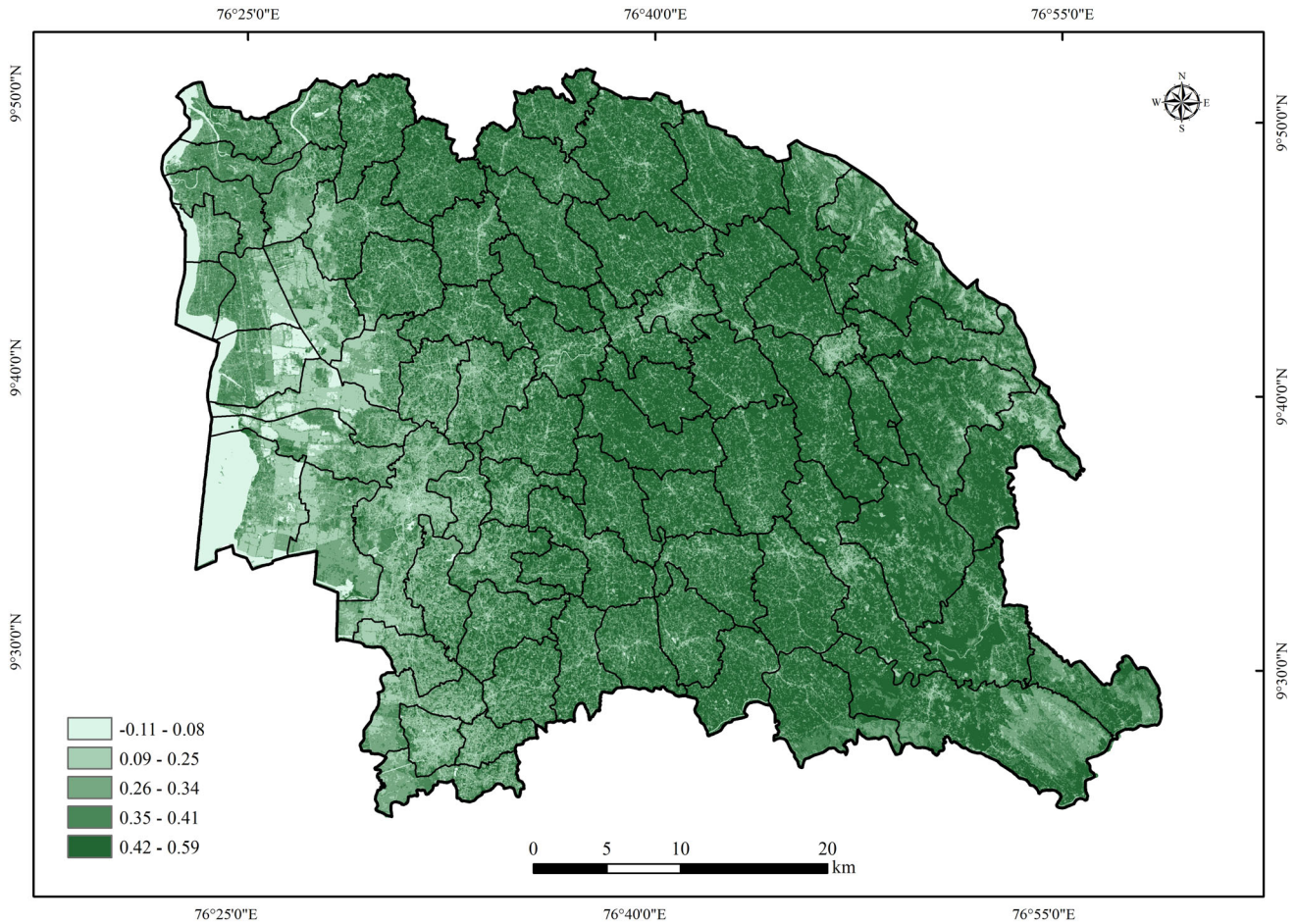

Fig. 7 Normalized Difference Vegetation Index (NDVI) of the study area. The highly urbanized Kottayam town is noteworthy in west-central region

3.1.10 Total population

Areas with a larger population will be more exposed to a hazard and the evacuation process may be challenging, making them more vulnerable (Tascón-González et al. 2020). The population of the study area ranges between 7029 and 55,374 (Fig. 8a) and is divided into five zones (7029–14,339, 14,340–20,752, 20,753–27,977, 27,978–38,445, and 38,446–55,374).

3.1.11 Number of households

As the rescue and evacuation processes will be much more complicated, the areas with a higher number of buildings will be more vulnerable than those with a lower number of buildings (Fernandez et al. 2016). The households in the study area range between 1706 and 14,366 (Fig. 8b) and are divided into five zones (1706–3556, 3557–4910, 4911–6952, 6953–9737, and 9738–14,366).

3.1.12 Literacy rate

A population's level and quality of education is a strong indicator of its vulnerability (Rasch 2016). Illiterates were thought to be more vulnerable because they lack the basic skills necessary to adapt to a risky situation (Deepak et al. 2020). The literacy rate of the study area ranges from 82.61 to 90.47% (Fig. 8c) and is categorized into five zones (82.61%, 82.62–87.66%, 87.67–88.63%, 88.64–89.61%, and 89.62–90.47%).

3.1.13 Building roof type

The roof of the buildings was categorized into different groups, viz., grass/thatch/bamboo/wood/mud, plastic/polythene, handmade tiles, machine-made tiles, burnt brick, stone/slate, G.I./metal/asbestos sheets, concrete, and others. Houses with concrete roofs will be more resistant to flooding. The majority of the houses in the study area have concrete roofs and hence, those houses were selected for the modelling. Houses other than concrete roofs will be

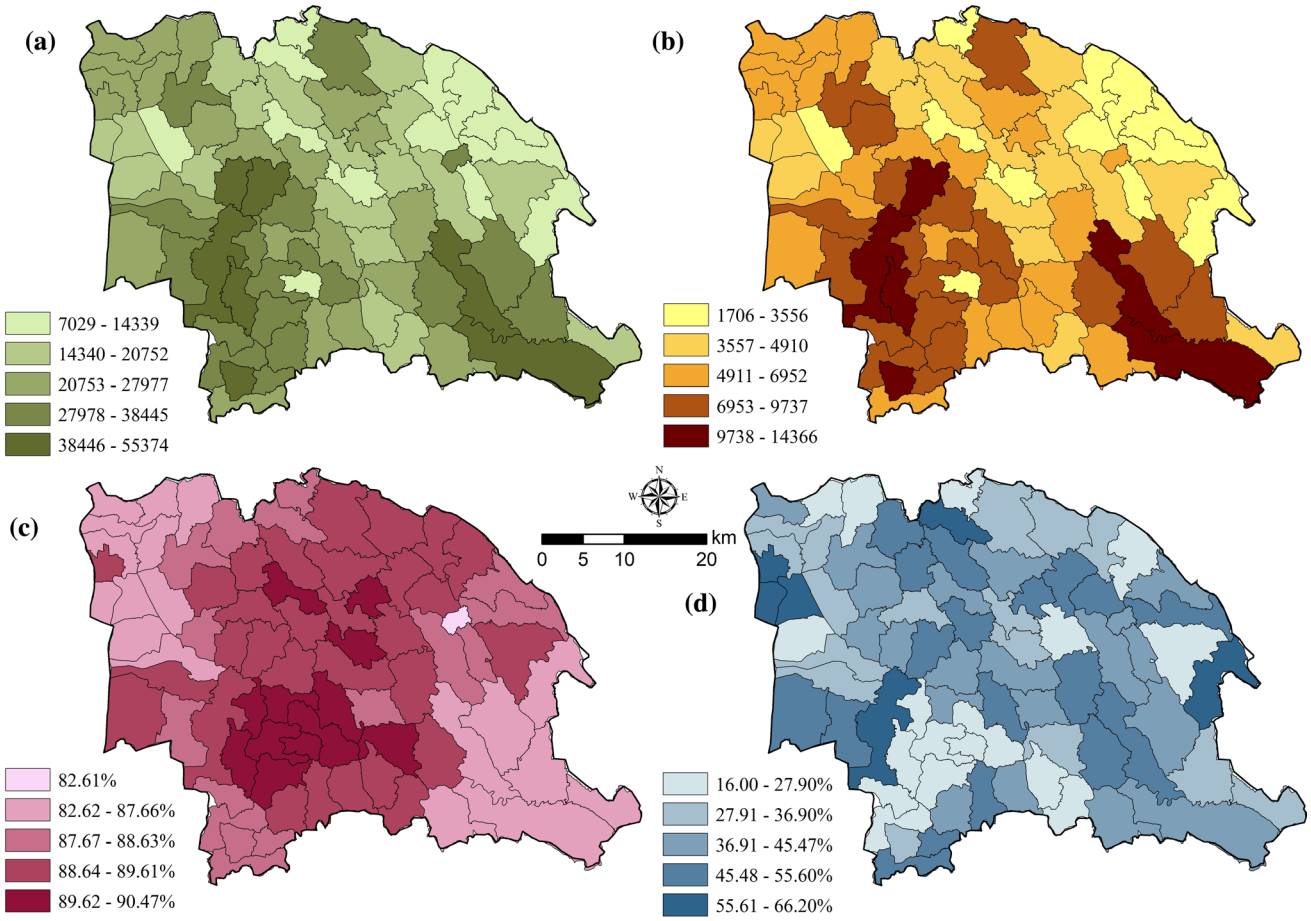

Fig. 8 **a**. Total population; **b**. No. of households; **c**. Literacy rate; **d**. Building roof type

more vulnerable to flooding. The percentage of buildings with concrete roofs ranges between 16.00 and 66.20% (Fig. 8d) and is categorized into five classes (16.00–27.90%, 27.91–36.90%, 36.91–45.47%, 45.48–55.60%, and 55.61–66.20%).

3.1.14 Building conditions

In the census data, the houses were categorized into three groups: good, liveable, and dilapidated. The dilapidated houses will be more prone to flooding. The percentage of dilapidated houses in the district ranges between 0.00 and 11.00% (Fig. 9a) and is grouped into five classes (0.00–1.40%, 1.41–3.20%, 3.21–5.00%, 5.01–7.20%, and 7.21–11.00%).

3.1.15 Household size

The larger the household size, the greater the number of people impacted and the severity of the damage, and also, they have to share the resources. (Deepak et al. 2020). In this study, only houses with five or more residents were selected. The percentage of houses with five or more residents ranges between 10.13 and 16.60% (Fig. 9b), and is categorized into five classes (10.13–11.16%, 11.17–12.06%, 12.07–12.68%, 12.69–14.10%, and 14.11–16.60%).

3.1.16 Child population

Children are particularly vulnerable to flood hazards as finding higher ground is more difficult for them and thus, increasing the likelihood of drowning-related fatalities (Rasch 2016). The child population is categorized into five classes: 7.11–7.90%, 7.91–8.51%, 8.52–9.16%, 9.17–10.18%, and 10.19–13.25% (Fig. 9c).

3.1.17 Marginalized population 1

Scheduled caste (SC) and scheduled tribe (ST) are among India's most socio-economically disadvantaged groups. In this study, marginalized population 1 represents SC, whereas 2 denotes ST category. Areas with a higher number of SC residents are therefore more vulnerable to

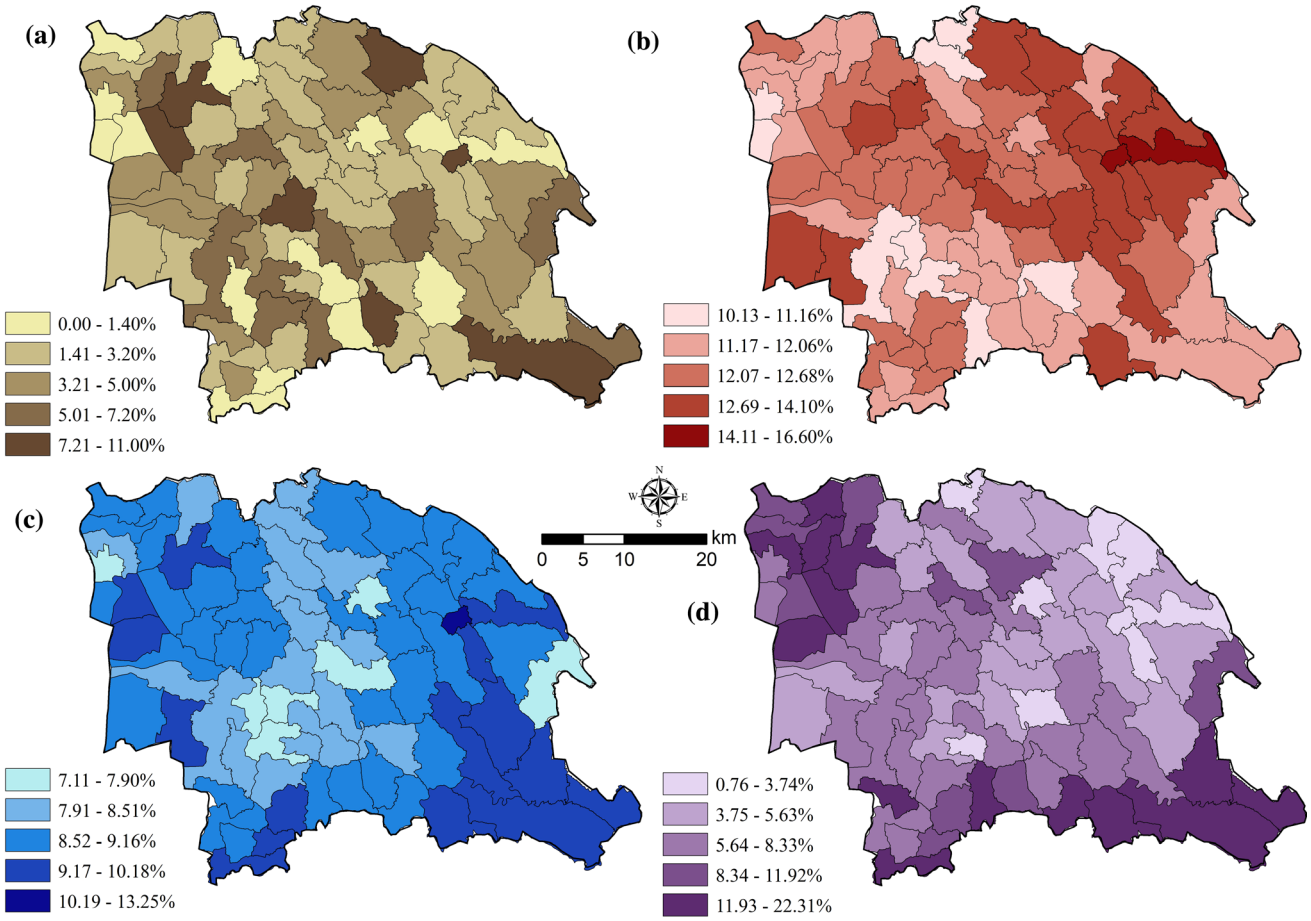

Fig. 9 **a**. Building condition; **b**. Household size; **c**. Child population; **d**. Marginalized population 1

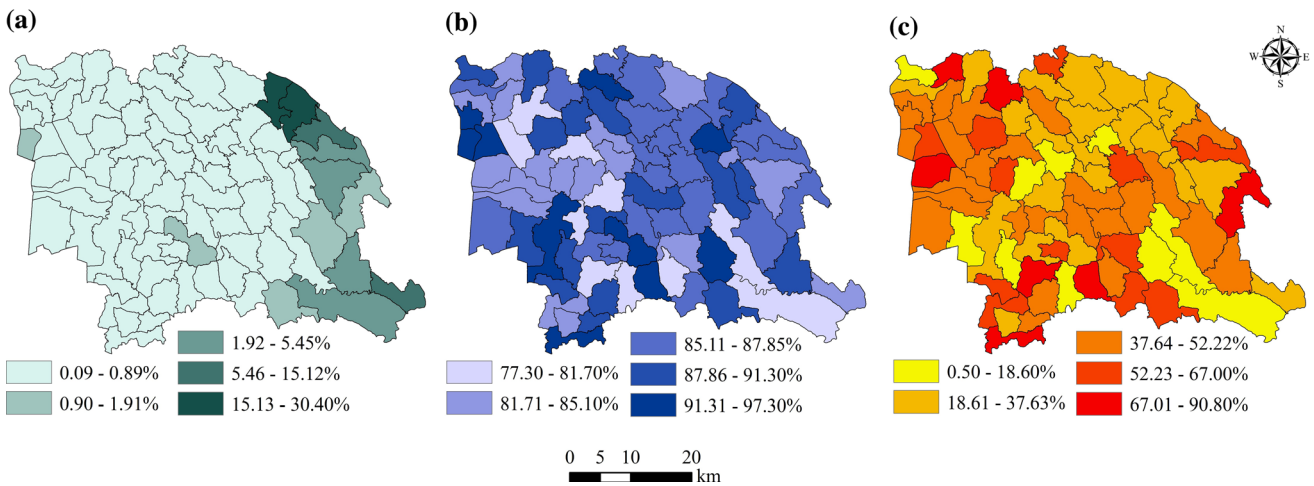

Fig. 10 **a** Marginalized population 2; **b** access to information; **c** building wall type

flooding. The percentage of the marginalized population 1 (SC) in the study area ranges from 0.76 to 22.31% (Fig. 9d) and is categorized into five: 0.76–3.74%, 3.75–5.63%, 5.64–8.33%, 8.34–11.92%, and 11.93–22.31%.

3.1.18 Marginalized population 2

As mentioned earlier, the ST population is a socio-economically weaker group in India. Hence, they are more vulnerable to flooding. The percentage of the marginalized

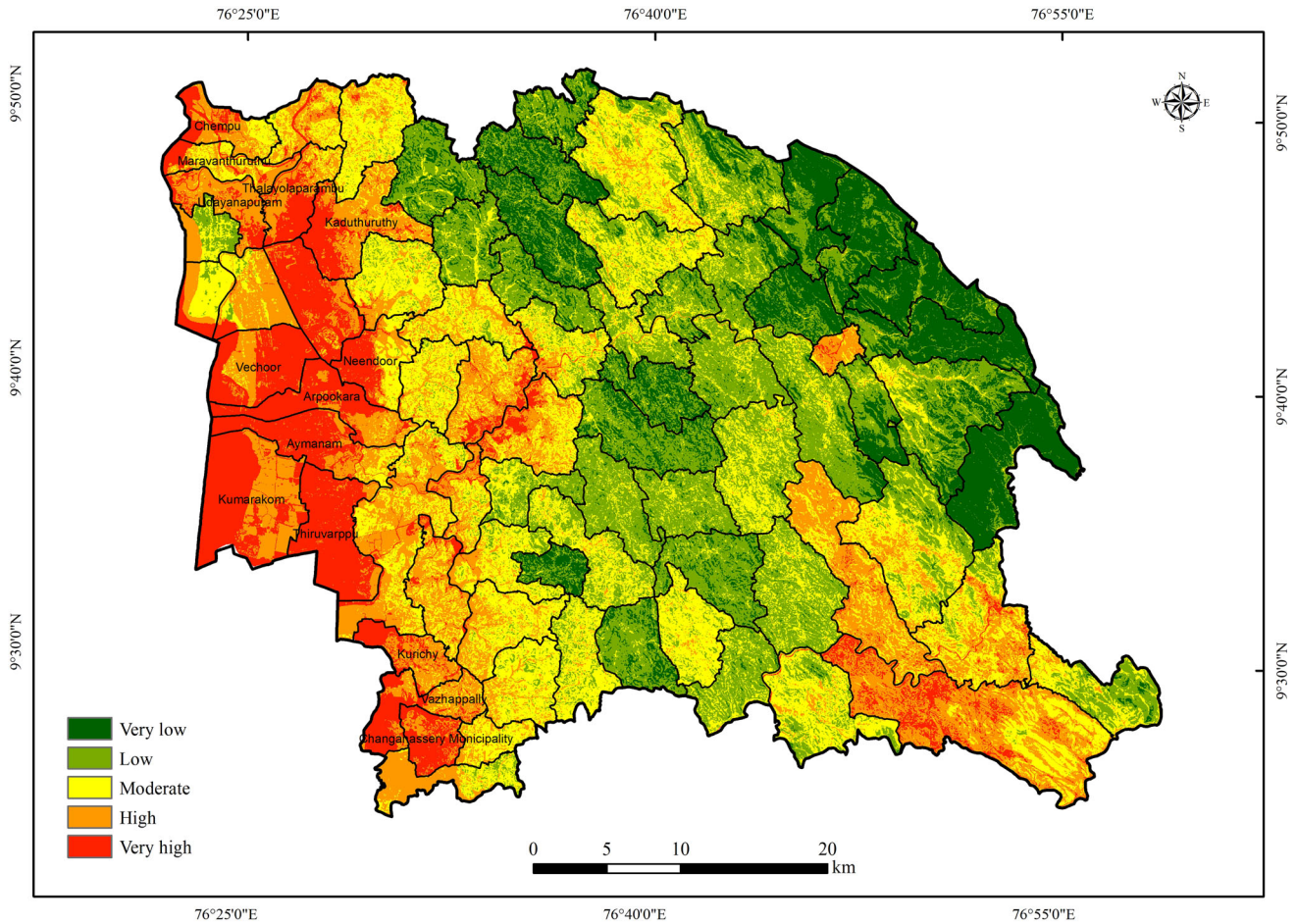

Fig. 11 Flood vulnerability: AHP method

population 2 (ST) in the study area ranges from 0.09 to 30.40% (Fig. 10a) and is categorized into five: 0.09–0.89%, 0.90–1.91%, 1.92–5.45%, 5.46–15.12%, and 15.13–30.40%.

3.1.19 Access to information

Vulnerability is influenced by one's capacity to access pertinent hazard information (Rasch 2016).Broadcasting of flood warnings through television and radio are frequent, and the community without access to television/radio will be more vulnerable to flooding. The percentage of people with access to information (television/radio) is categorized into five: 77.30–81.70%, 81.71–85.10%, 85.11–87.85%, 87.86–91.30%, and 91.31–97.30% (Fig. 10b).

3.1.20 Building wall type

The strength of a house's walls will determine how vulnerable it is to flood damage (Rasch 2016). The materials for the wall were grouped into grass/thatch/bamboo, plastic/polythene, mud/unburnt brick, wood, stone not packed with mortar, stone packed with mortar, G.I./metal/asbestos sheets, burnt brick, concrete, and others. Houses with walls made of burnt bricks and concrete are more resistant to flooding. The majority of the houses in the study area have walls made of burnt bricks and concrete and hence, those houses were selected for the modelling. The walls constructed using materials other than burnt bricks and concrete will be more vulnerable to flooding. The percentage of buildings with walls made of burnt bricks and concrete ranges between 0.50 and 90.80% (Fig. 10c) and is categorized into five classes (0.50–18.60%, 18.61–37.63%, 37.64–52.22%, 52.23–67.00%, and 67.01–90.80%).

3.2 Flood vulnerability

The flood vulnerability of Kottayam district is depicted in Figs. 11 and 12. The very high flood vulnerable zones are mainly confined to the western portion of the study area. This is due to the high to very high physical-environmental vulnerability and socio-economic vulnerability of this area. According to this study, a total of 12.29% and 11.81% of the district are categorized into very highly vulnerable

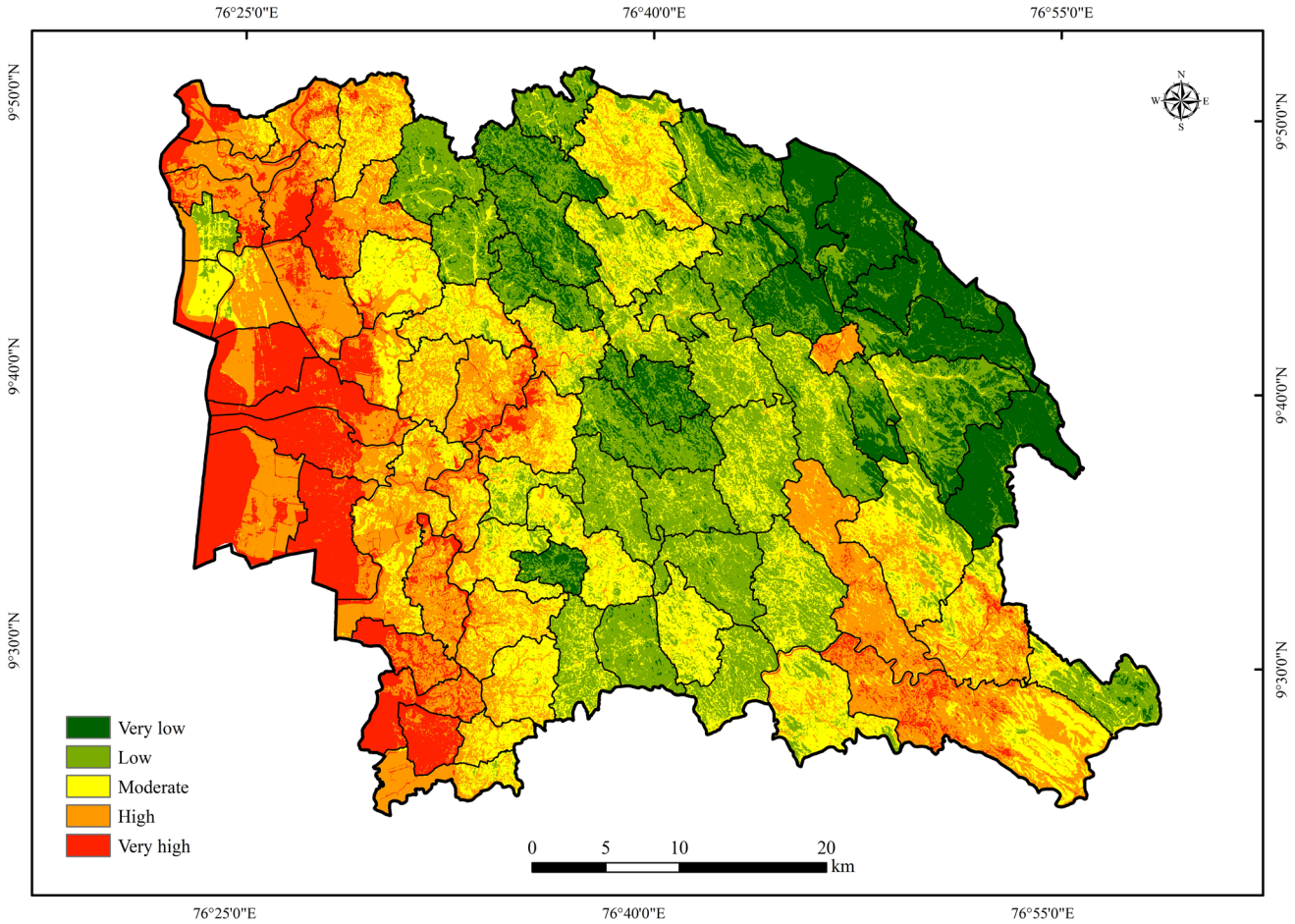

Fig. 12 Flood vulnerability: F-AHP method

Table 12 Area and percentage of flood vulnerable zones

Vulnerable zones	AHP method		F-AHP method	
	Area (sq. km)	Percentage of the area of the vulnerable zones	Area (sq. km)	Percentage of the area of the vulnerable zones
Very low	302.28	13.69	290.79	13.17
Low	591.08	26.77	577.39	26.15
Moderate	587.11	26.59	553.55	25.07
High	455.95	20.65	525.50	23.80
Very high	271.36	12.29	260.77	11.81
Total	2208	100	2208	100

zones by the AHP and F-AHP models, respectively (Table 12). The ROC curve analysis proved that both the models are effective, with an outstanding AUC value of 0.94 (Fig. 13). However, the AHP model (0.946) provided slightly better results than the F-AHP model (0.943). According to the vulnerability created using the AHP model, the panchayats (Hamlet level LSG), namely Neendoor, Vechoor, Aymanam, Arpookara, Chempu, Thalayolaparambu, Kumarakom, Thiruvarppu, Kaduthuruthy, Vazhappally, Kurichy, Udayanapuram, and Maravanthuruthu, and the municipality of Changanassery, are the very high flood vulnerable zones. From the study, it was found that a major portion of the very high flood

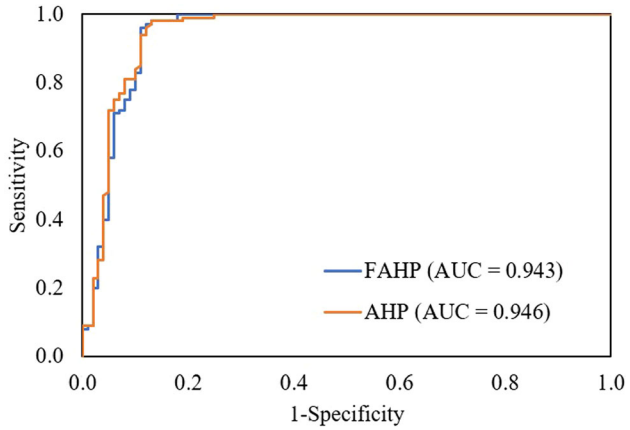

Fig. 13 The ROC curves: flood vulnerability

vulnerable zone is agricultural land, followed by wetlands (Table 13).

3.3 Physical-environmental vulnerability (PEV)

The vulnerability maps for the physical-environmental indicators are depicted in Figs. 14 and 15. Major portions of the high and very highly vulnerable zones are confined to the western part of the study area. The area of each vulnerable zone is shown in Table 14. From the modelling, it is confirmed that slope, soil, LULC, stream density, and geomorphology are the major causative factors. The high and very high vulnerable areas have lower slopes, clayey soil, agricultural land (paddy fields), lowest stream density, and are coastal plains. A considerable percentage of the area of the high and very highly vulnerable zones has lower NDVI values, higher WRI, MNDWI, and NDBI values. Thus, it is proved beyond doubt that all the factors selected for the modelling are relevant. The AUC scores of 0.88 and 0.91 for the vulnerability maps created using the AHP and F-AHP methods confirm that the results are excellent and outstanding for these two models, respectively (Fig. 16). The AUC score of 0.91 proves that the F-AHP method has better prediction accuracy than the AHP method. According to the map created using the F-AHP method, the high and very high vulnerable zones together constitute 20.73% of the district.

3.4 Socio-economic vulnerability (SEV)

Figures 17 and 18 show the vulnerability maps for the socio-economic indicators. The ROC curve analysis (Fig. 19) proved that the F-AHP model (with an AUC score of 0.953) is better than the AHP model (with an AUC score of 0.92). Hence, the F-AHP model was selected as the best model. Both the models provided outstanding results. According to the vulnerability map created using the F-AHP model, panchayats viz. Kurichy, Vazhappally, Kaduthuruthy, Kanjirappally, Mundakkayam, Erumely and Changanasserry, and Erattupetta municipalities (middle level LSG) are very highly vulnerable. Most of the highly vulnerable LSGs are concentrated in the low-lying regions of the district. The highly and very highly vulnerable zones have lower literacy rates, lower access to information, a comparatively higher child population, larger household sizes, larger MP2, and a lower percentage of houses with concrete roofs. The low socio-economic conditions of the people living in the high and very high vulnerable areas impact egregiously on their lives and property as a result of a natural disaster. Even a frail disaster might lead to great loss and damage to society and its people.

Table 13 Land use/land cover classes in each flood vulnerable zones

Vulnerable zones	AHP method								F-AHP method							
	Area in sq. km								Area in sq. km							
	GL	PL	BA	WB	WL	AL	EF	FP	GL	PL	BA	WB	WL	AL	EF	FP
Very low	6.38	210.63	6.29	0.20	1.39	0.51	2.62	74.26	7.03	197.51	5.73	0.19	0.00	0.38	4.15	75.80
Low	2.95	487.58	33.56	0.61	2.82	6.47	6.33	50.76	2.42	477.80	33.96	0.61	0.00	6.46	8.33	47.81
Moderate	3.13	432.62	73.31	1.30	0.06	31.29	7.28	38.12	2.04	407.03	63.52	1.25	0.04	28.45	8.89	42.33
High	19.10	205.13	88.48	5.84	7.93	105.94	3.81	20.53	17.72	254.78	94.15	6.08	9.61	117.74	2.47	22.95
Very high	9.89	16.63	25.20	18.86	60.05	**138.71**	0.00	2.02	11.20	14.45	28.45	18.64	57.70	**129.62**	0.00	0.71

Where GL = Grassland, PL = Plantation, BA = Built-up area, WB = Water body, WL = Wetland, AL = Agricultural land, EF = Evergreen Forest, and FP = Forest plantation

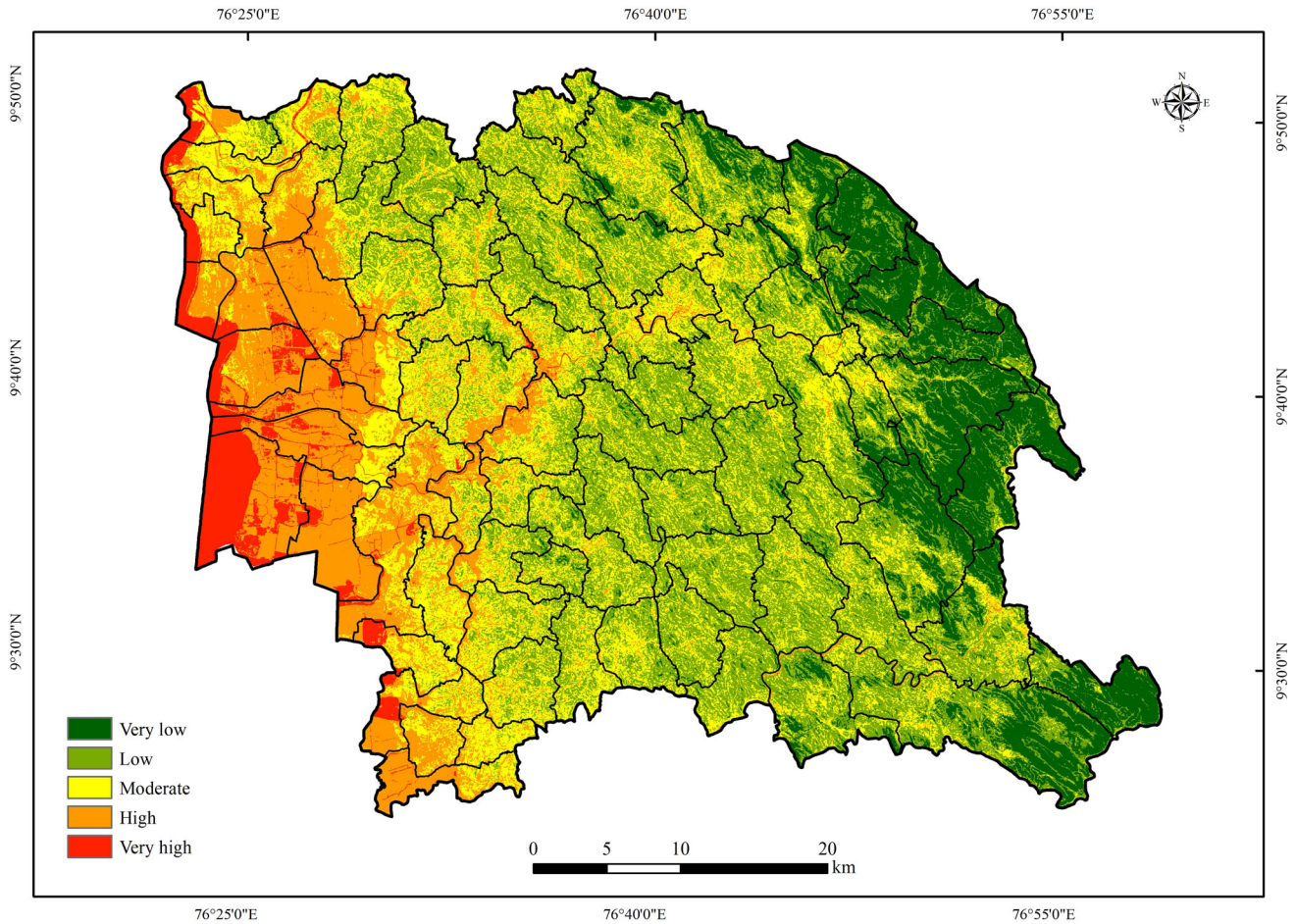

Fig. 14 Physical-environmental vulnerability: AHP method

4 Discussion

The vulnerability studies, melding the PEV and SEV indicators, reveal that AHP and F-AHP as ideal methods. Through the use of the consistency measure, the AHP model improves the decision-making process (Olson 1988). During pairwise comparisons of factors, AHP allows for a certain level of inconsistency (Afolayan et al. 2020). Fuzzy logic, a method based on possibility theory (Thompson et al. 2012), can be highly useful in describing complex systems, especially those containing ambiguities and non-linearities (Chanal et al. 2021). The fuzzy logic method is advantageous since it is simple and easy to understand, and it does not require a large amount of data for training purposes. Many problems involving imprecise and uncertain data can be solved using the fuzzy logic method (Afolayan et al. 2020). F-AHP is an AHP method based on fuzzy logic theory (Putra et al. 2018). F-AHP will be used to address AHP's inability to handle imprecision and subjectivity in judgments (Carnero 2020; Liu et al. 2020). A few previous studies (cf. Ali et al. 2019; Feloni et al. 2020) compared the AHP versus FR models, and the AHP versus F-AHP models for flood vulnerability modelling. Moreover, the reliability of using such models depends on the factors that are selected for the analysis. The study conducted by Feloni et al. (2020) hasn't considered the SEV indicators. Deepak et al. (2020) applied the AHP method and Random Forest models for demarcating the flood vulnerable zones of a municipality in the Ernakulam district (India). They considered both PEV and SEV indicators, but the study was limited to a smaller area. The present study found that the F-AHP model is more effective than the AHP model for the assessment of PEV and SEV, whereas the AHP model was found to be slightly better than the F-AHP for the flood vulnerability assessment. Akshaya et al. (2021), Khashei-Siuki et al. (2020), and Tripathi et al. (2021) also found that the F-AHP model is effective than the AHP model.

According to the PEV modelling, very high and high vulnerable zones have lower slopes, clayey soil, agricultural land, the lowest stream density, and are coastal plains. Lower NDVI, higher WRI, MNDWI, and NDBI values are found in a significant percentage in these zones. The clayey

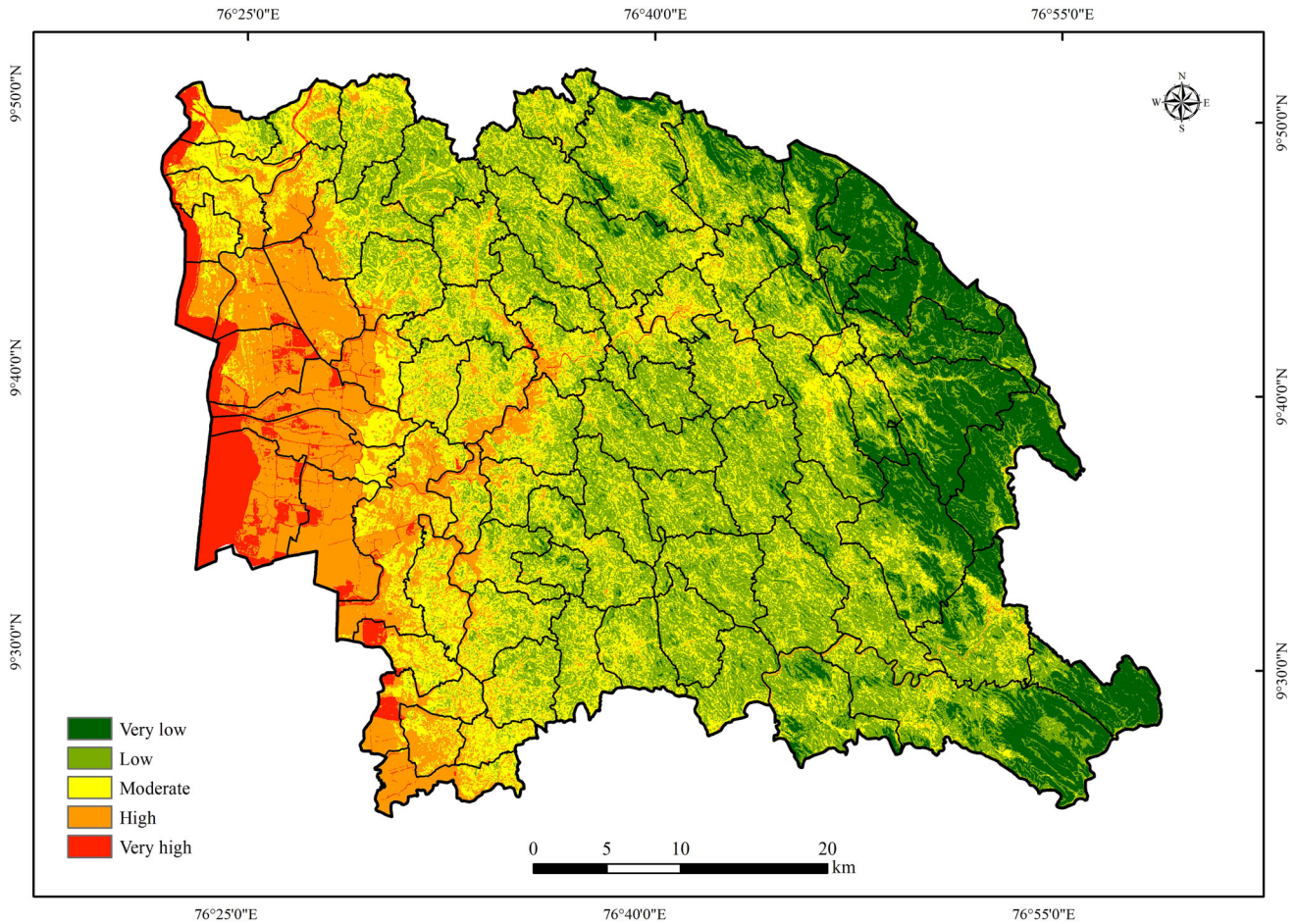

Fig. 15 Physical-environmental vulnerability: F-AHP method

Table 14 Area and percentage of vulnerable zones (Physical-environmental)

Vulnerable zones	AHP method		F-AHP method	
	Area (sq. km)	Percentage of the area of the vulnerable zones	Area (sq. km)	Percentage of the area of the vulnerable zones
Very low	300.73	13.62	296.53	13.43
Low	771.70	34.95	787.82	35.68
Moderate	664.83	30.11	665.93	30.16
High	375.36	17.00	368.08	16.67
Very high	95.38	4.32	89.64	4.06
Total	2208	100	2208	100

soil with poor infiltration capacity and lower slopes are ideal conditions for flooding. This observation concurs with the findings of Samanta et al. (2018), where they found that regions with poorly drained soil and lower slopes (0–5°) are the primary reasons for flooding. The low-lying, flood-prone areas of the Kottayam district are agricultural land (especially paddy fields) and coastal plains. These geomorphic/physiographic conditions usually facilitate flooding.

Based on the SEV modeling, highly and very highly vulnerable zones have lower literacy rates, lower access to information, a comparatively higher child population, larger household sizes, larger marginalized population 2, and a smaller percentage of dwellings with concrete roofs.

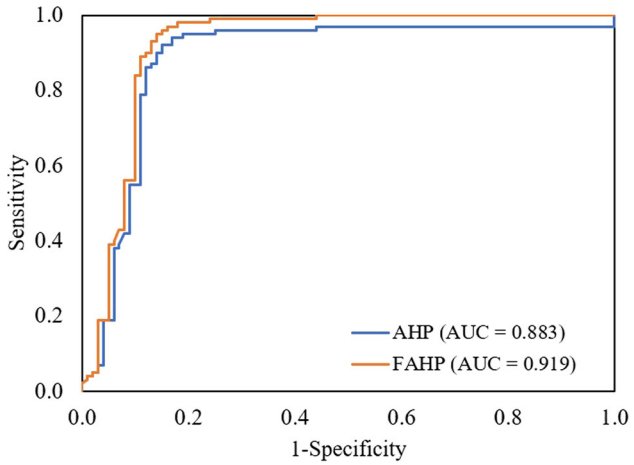

Fig. 16 The ROC curves: physical-environmental vulnerability

Literacy can have a direct and indirect influence on disaster vulnerability (Hoffmann and Blecha 2020), which is defined as the ability to foresee, cope with, resist, and recover from natural hazards. Literacy can directly influence the knowledge, capabilities, skills, and perceptions acquired by individuals that allow them to effectively prepare for and deal with disaster shocks (Hoffmann and Blecha 2020). Indirectly, literacy makes individuals and households have indirect access to material, informational, and social resources, which can assist in reducing disaster vulnerability (Hoffmann and Blecha 2020). The findings of this study concur those of Sam et al. (2017), where they identified low literacy rates and weak housing structures are the primary causes for flood vulnerability. According to Peek (2008), children are psychologically vulnerable and may suffer from post-traumatic stress disorder during such disasters. They are also physically vulnerable to death, injury, illness, and abuse, and disasters often impair or delay their educational progress (Peek 2008). Moreover, the lack of financial resources of the marginalized populations to recover from disasters, are regarded as vulnerable to disasters (Fucile-Sanchez and Davlasheridze 2020).

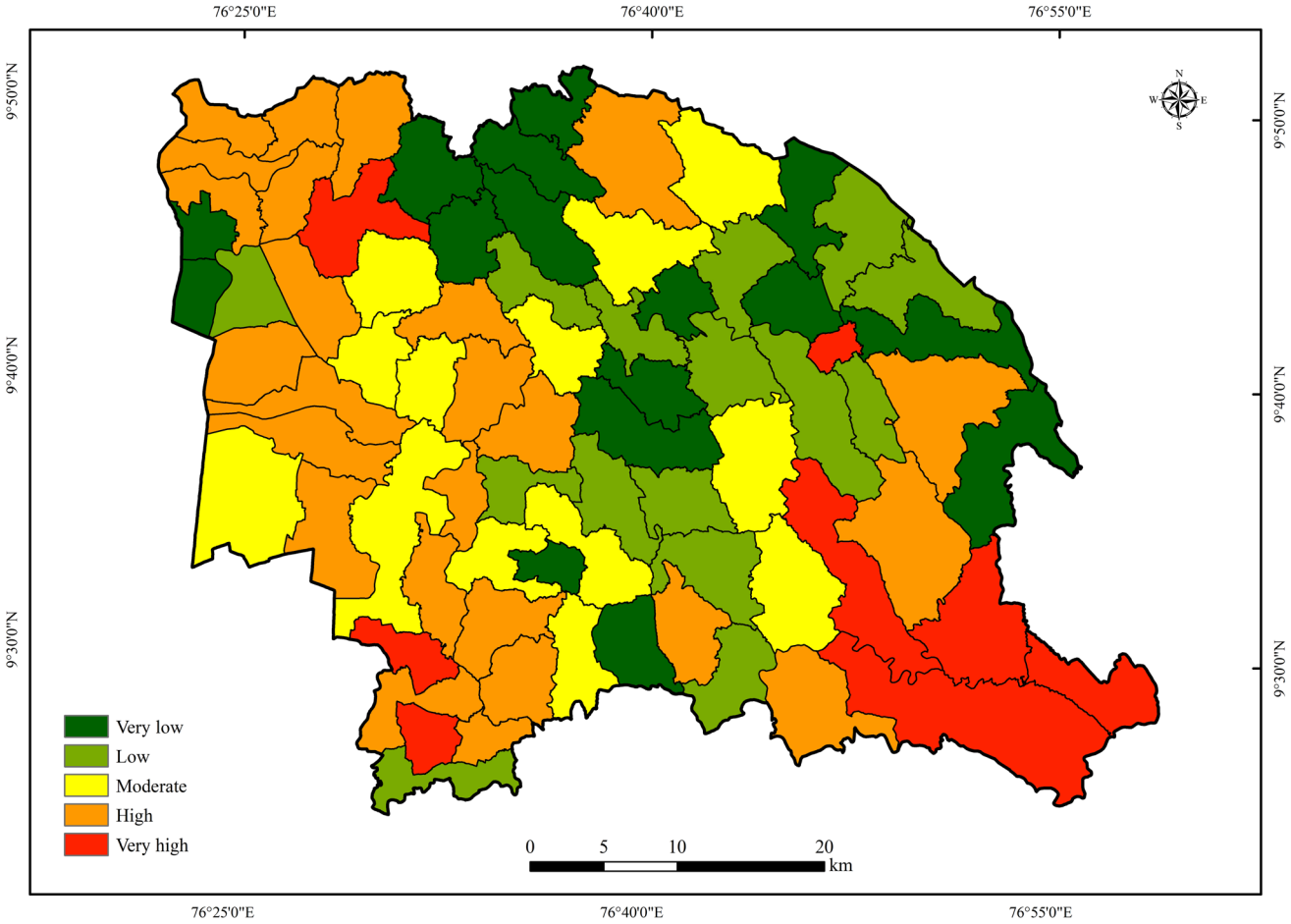

Fig. 17 Socio-economic vulnerability: AHP method

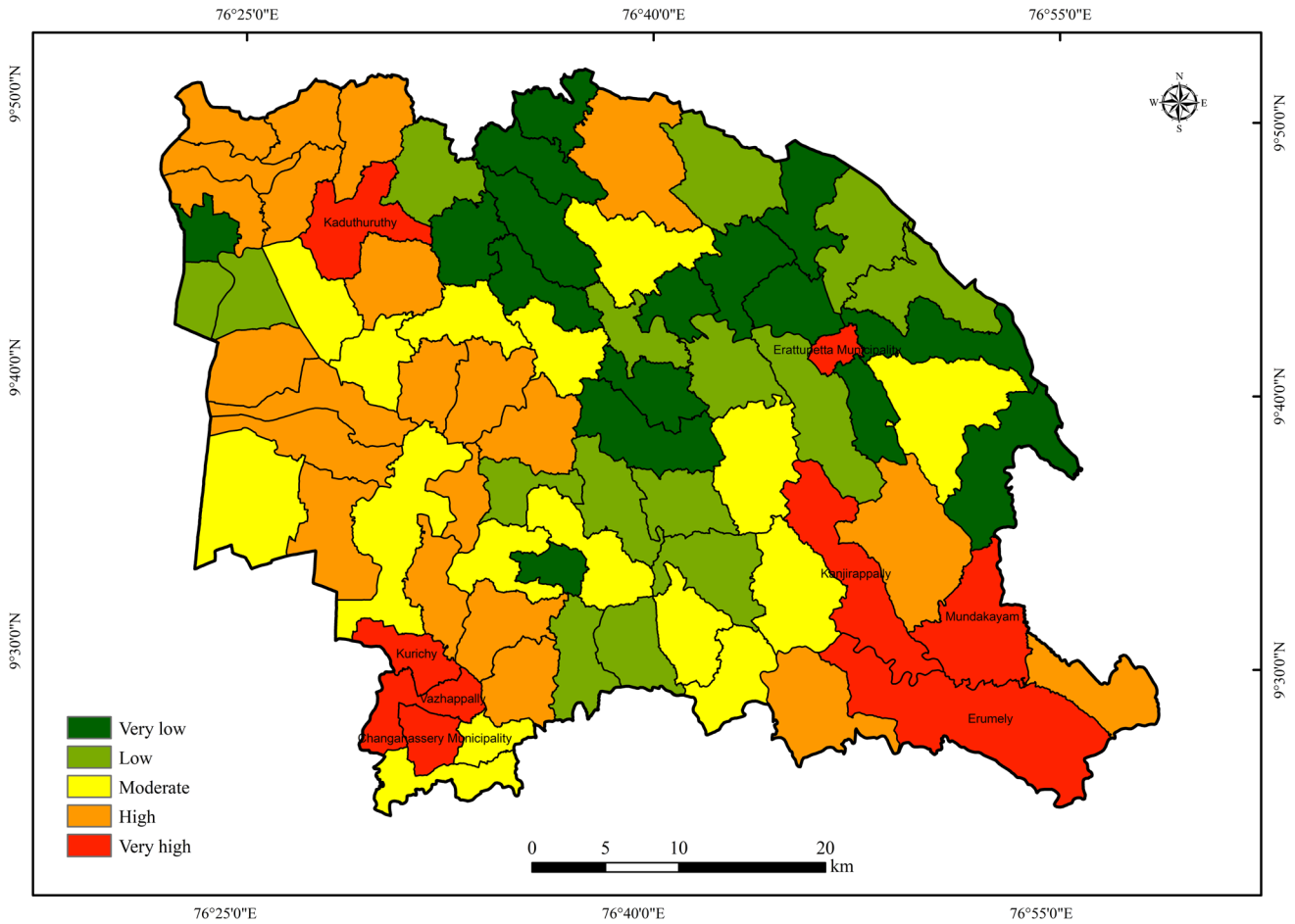

Fig. 18 Socio-economic vulnerability: F-AHP method

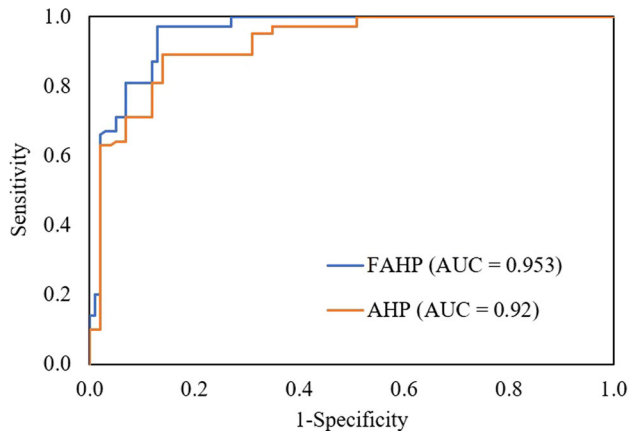

Fig. 19 The ROC curves: socio-economic vulnerability

4.1 Advantages of this or similar studies

The increasing frequency of flood occurrences due to heavy rainfall, and subsequent overflowing and discoursing of rivers in the study area led to heavy financial hardship and distress among individuals and governments. Usually, most countries have contingency funds to face any kind of disastrous situation. In the case of India, from 2006 onwards, both the center (Federal Government) and the states have established the National Disaster Response Fund (NDRF) and the State Disaster Response Fund (SDRF), respectively, as per the enactment of the Disaster Management Act 2005 by Parliament. These funds are only utilized as per the list of items and the norms of relief assistance that are included in its guidelines. As per the norms of the NDRF and SDRF, the government of India is paying 0.4 million INR for the death of a person due to flooding; ∼ 0.1 million INR for a fully damaged house (in plain areas); and ∼ 0.04 million INR/hectare for substantial loss of agricultural land (only to small and marginal farmers) (https://sdma.kerala.gov.in/sdrf-norms/). These assistance funds are significantly insufficient when compared to the actual value of the loss or damage to life and property. As the relief assistance was inadequate, the Kerala government increased the amount for some of the items. This additional fund is allocated from the Chief Ministers' Disaster Relief Fund (CMDRF). Hence, the exchequer is spending an enormous amount of money on

flood damage. Thus, this sort of study will help in identifying areas vulnerable to flooding and taking precautionary measures so that the effects of flooding can be minimized. The huge amount of money saved through this can be utilized for implementing mitigation measures. Priority areas that require mitigation measures can also be identified through studies of this nature.

Akin to this, measures that are adopted in developed countries like the US, which do not provide any assistance to people for flood-related deaths, injuries, and damage (agriculture loss, infrastructure loss, and so on) from their budget, rather pay through flood insurance, and such options should also be explored by developing countries like India. For example, the Federal Emergency Management Agency (FEMA) manages the National Flood Insurance Program (NFIP) for the US, which is provided to the public by a network of more than 50 insurance firms (https://www.fema.gov/flood-insurance). Hence, implementation of disaster risk financing strategies is of utmost importance to reduce the burden of the government. The majority of the people in Kerala have a higher income than the national average, where the replacement cost of the average house would be more than 4–5 million INR (UNDP 2018). Implementation of a suitable disaster risk financing strategy is of utmost importance to society. Presently, the disaster risk financing schemes available in the state are mostly ex-post mechanisms such as budget reallocations and SDRF/NDRF, rather than ex-ante in nature, like insurance and catastrophic bonds (Government of Kerala 2019b). Hence, by implementing new flood insurance schemes with the support of private insurance companies, a huge amount of money spent from the budget can be saved and utilized for flood mitigation measures.

5 Conclusions

Before delving into the significance of this study, the major constrains are: this study utilized the 2011 census data, which is the only available valid data published by the Indian government. The next census data, scheduled for 2021, is overdue in lieu of the COVID-19 pandemic. Due to a lack of authentic data on the elderly population, this was not considered in this study. The data on the elderly population is very relevant for flood vulnerability assessment, as the elderly population is more vulnerable to flooding. Also, due to a lack of an adequate number of weather stations, the rainfall (the triggering factor) data was not considered in this modelling. Moreover, the gridded data from the India Meteorological Department (IMD) is available for free, but it has a lower resolution ($\sim$25 km).

And the following are the study's key findings:

- The AHP and F-AHP methods classified 12.29% and 11.81%, respectively, of the study area as very highly vulnerable to floods.
- Soil is the most important PEV indicator, followed by LULC, slope angle, stream density, and geomorphology.
- A large portion of the high and very high flood vulnerability zones is agricultural land. As a result, the economic loss connected with agricultural land and crop destruction will be significant.
- Lower literacy rates, lower access to information, a disproportionately higher child population, larger household size, a larger SC population, and a lower number of dwellings with concrete roofs characterize the high and very high flood vulnerable zones.
- With an AUC value greater than 0.94, both the AHP and the F-AHP methods are outstanding in identifying flood-vulnerable zones.
- The F-AHP method (AUC values: 0.919 and 0.953) outperforms the AHP method (AUC values: 0.883 and 0.92) for PEV and SEV modelling, while the AHP method (AUC value: 0.946) slightly outperforms the F-AHP method (AUC value: 0.943) for flood vulnerability modelling.

According to this study, both methods were found to be effective in mapping flood vulnerability and can be adapted to other locations with similar physiographical settings. The generated flood vulnerability maps will assist land-use planners in identifying critical locations in Kottayam district, allowing them to implement effective mitigation measures to prevent loss of life, infrastructure, and property, as well as avoid development in these areas.

Based on the findings of the present study, the following recommendations are made:

- Implement a suitable disaster risk financing strategy and flood insurance schemes.
- Conduct household survey-based studies to assess the willingness of communities in flood vulnerable and flood-affected areas to pay for flood insurance.
- Install automated weather stations or automated rain gauges at the village/LSG level. This will enhance the monitoring of rainfall and provide more accurate weather predictions.
- Clear debris, aquatic weed plants like water hyacinth (*Eichhornia crassipes*), and other obstructions from the stream channels and widen the stream channels so as to drain out the excess rain water.
- Ban construction on the river course and floodplains, implement zoning of the areas based on the flood hazard level, and stop development activities that block the stream channels.

- Make available high-resolution DEM (such as LiDAR data or drone images) to create high-resolution flood susceptibility maps for further micro-scale studies.

Acknowledgements This study was supported by a research centre in Iran (Grant No. 54RCTR763542). The authors would like to express their gratitude to the editor and anonymous reviewers for their insightful comments on earlier versions of the manuscript.

Funding This study was supported by a research centre in Iran (Grant No. 54RCTR763542).

Availability of data and materials The datasets generated during and/or analysed during the current study are available from the corresponding author on reasonable request.

Declarations

Conflict of interest The authors have no conflicts of interest to declare.

Ethical approval This article does not contain any studies with human participants or animals performed by any of the authors.

Informed consent Not applicable.

References

Abebe Y, Kabir G, Tesfamariam S (2018) Assessing urban areas vulnerability to pluvial flooding using GIS applications and Bayesian belief network model. J Clean Prod 174:1629–1641. https://doi.org/10.1016/j.jclepro.2017.11.066

Abu Reza M, Islam T, Talukdar S, Mahato S, Kundu S, Eibek KU, Pham QB, Kuriqi A, Linh NTT (2021) Flood susceptibility modelling using advanced ensemble machine learning models. Geosci Front 12(3):101075. https://doi.org/10.1016/j.gsf.2020.09.006

Afolayan AH, Ojokoh BA, Adetunmbi AO (2020) Performance analysis of fuzzy analytic hierarchy process multi-criteria decision support models for contractor selection. Sci Afr. https://doi.org/10.1016/j.sciaf.2020.e00471

Ahmed B (2015) Landslide susceptibility mapping using multi-criteria evaluation techniques in Chittagong metropolitan area, Bangladesh. Landslides 12:1077–1095. https://doi.org/10.1007/s10346-014-0521-x

Ajin RS, Krishnamurthy RR, Jayaprakash M, Vinod PG (2013) Flood hazard assessment of Vamanapuram river basin, Kerala, India: an approach using remote Sensing & GIS techniques. Adv Appl Sci Res 4(3):263–274

Ajin RS, Loghin AM, Vinod PG, Jacob MK (2019) Flood hazard zone mapping in the tropical Achankovil river basin in Kerala: a study using remote sensing data and geographic information system. J Wetlands Biodiv 9:45–58

Akshaya M, Danumah JH, Saha S, Ajin RS, Kuriakose SL (2021) Landslide susceptibility zonation of the Western Ghats region in Thiruvananthapuram district (Kerala) using geospatial tools: a comparison of the AHP and Fuzzy-AHP methods. Saf Extreme Environ 3:181–202. https://doi.org/10.1007/s42797-021-00042-0

Ali SA, Khatun R, Ahmad A, Ahmad SN (2019) Application of GIS-based analytic hierarchy process and frequency ratio model to flood vulnerable mapping and risk area estimation at Sundarban region, India. Model Earth Syst Environ 5:1083–1102. https://doi.org/10.1007/s40808-019-00593-z

Amrutha K, Danumah JH, Nikhil S, Saha S, Rajaneesh A, Mammen PC, Ajin RS, Kuriakose SL (2022) Demarcation of forest fire risk zones in silent valley national park and the effectiveness of forest management regime. J Geovisual Spat Anal. https://doi.org/10.1007/s41651-022-00103-3

Ayhan MB (2013) A fuzzy AHP approach for supplier selection problem: a case study in a gear motor company. Int J Manag Value Supply Chains 4(3):11–23. https://doi.org/10.5121/ijmvsc.2013.4302

Buckley JJ (1985) Fuzzy hierarchical analysis. Fuzzy Sets Syst 17(1):233–247

Carnero MC (2020) Fuzzy multicriteria models for decision making in gamification. Mathematics. https://doi.org/10.3390/math8050682

Chadsuthi S, Chalvet-Monfray K, Wiratsudakul A, Modchang C (2021) The effects of flooding and weather conditions on leptospirosis transmission in Thailand. Sci Rep. https://doi.org/10.1038/s41598-020-79546-x

Chanal D, Steiner NY, Petrone R, Chamagne D, Péra MC (2021) Online diagnosis of PEM fuel cell by fuzzy C-means clustering. Ref Module Earth Syst Environ Sci. https://doi.org/10.1016/B978-0-12-819723-3.00099-8

Ching YC, Lee YH, Toriman ME, Abdullah M, Yatim BB (2015) Effect of the big flood events on the water quality of the Muar River, Malaysia. Sustain Water Resour Manag 1:97–110. https://doi.org/10.1007/s40899-015-0009-4

Chou SW, Chang YC (2008) The implementation factors that influence the ERP (enterprise resource planning) benefits. Decis Support Syst 46(1):149–157

Chukwuma EC, Okonkwo CC, Ojediran JO, Anizoba DC, Ubah JI, Nwachukwu CP (2021) A GIS based flood vulnerability modelling of Anambra State using an integrated IVFRN-DEMATEL-ANP model. Heliyon 7(9):e08048. https://doi.org/10.1016/j.heliyon.2021.e08048

Crabtree A (2013) Questioning psychosocial resilience after flooding and the consequences for disaster risk reduction. Soc Indic Res 113:711–728. https://doi.org/10.1007/s11205-013-0297-8

Dandapat K, Panda GK (2017) Flood vulnerability analysis and risk assessment using analytical hierarchy process. Model Earth Syst Environ 3:1627–1646. https://doi.org/10.1007/s40808-017-0388-7

Danumah JH, Odai SN, Saley BM, Szarzynski J, Thiel M, Kwaku A, Kouame FK, Akpa LY (2016) Flood risk assessment and mapping in Abidjan district using multi-criteria analysis (AHP) model and geoinformation techniques, (cote d'ivoire). Geoenviron Dis. https://doi.org/10.1186/s40677-016-0044-y

Deepak S, Rajan G, Jairaj PG (2020) Geospatial approach for assessment of vulnerability to flood in local self-governments. Geoenviron Dis. https://doi.org/10.1186/s40677-020-00172-w

Department of Mining and Geology (2016) District survey report of minor minerals (except river sand) – Kottayam district. Government of Kerala

Desalegn H, Mulu A (2020) Flood vulnerability assessment using GIS at Fetam watershed, upper Abbay basin. Ethiopia Heliyon. https://doi.org/10.1016/j.heliyon.2020.e05865

Donnini M, Napolitano E, Salvati P, Ardizzone F, Bucci F, Fiorucci F, Santangelo M, Cardinali M, Guzzetti F (2017) Impact of event landslides on road networks: a statistical analysis of two Italian case studies. Landslides 14:1521–1535. https://doi.org/10.1007/s10346-017-0829-4

Duan Y, Xiong J, Cheng W, Wang N, Li Y, He Y, Liu J, He W, Yang G (2021) Flood vulnerability assessment using the triangular fuzzy number-based analytic hierarchy process and support

vector machine model for the belt and road region. Nat Hazards. https://doi.org/10.1007/s11069-021-04946-9

Eskandari S, Miesel JR (2017) Comparison of the fuzzy AHP method, the spatial correlation method, and the Dong model to predict the fire high-risk areas in Hyrcanian forests of Iran. Geomat Nat Haz Risk 8(2):933–949. https://doi.org/10.1080/19475705.2017.1289249

Feloni E, Mousadis I, Baltas E (2020) Flood vulnerability assessment using a GIS-based multi-criteria approach: the case of Attica region. J Flood Risk Manag. https://doi.org/10.1111/jfr3.12563

Feng B, Zhang Y, Bourke R (2021) Urbanization impacts on flood risks based on urban growth data and coupled flood models. Nat Hazards 106:613–627. https://doi.org/10.1007/s11069-020-04480-0

Fernandez P, Mourato S, Moreira M, Pereira L (2016) A new approach for computing a flood vulnerability index using cluster analysis. Phys Chem Earth Parts a/b/c 94:47–55. https://doi.org/10.1016/j.pce.2016.04.003

Franzke CLE, Torelló i Sentelles H (2020) Risk of extreme high fatalities due to weather and climate hazards and its connection to large-scale climate variability. Clim Change 162:507–525. https://doi.org/10.1007/s10584-020-02825-z

Fucile-Sanchez E, Davlasheridze M (2020) Adjustments of socially vulnerable populations in Galveston County Texas USA following Hurricane Ike. Sustainability. https://doi.org/10.3390/su12177097

Gessesse AA, Melesse AM (2019) Chapter 8 - Temporal relationships between time series CHIRPS-rainfall estimation and eMODIS-NDVI satellite images in Amhara Region, Ethiopia. In: Melesse AM, Abtew W, Senay G (Eds) Extreme hydrology and climate variability, Elsevier, pp 81–92. https://doi.org/10.1016/B978-0-12-815998-9.00008-7

Global Natural Disaster Assessment Report (2020) Academy of Disaster Reduction and Emergency Management, Ministry of Emergency Management - Ministry of Education, National Disaster Reduction Center of China, Ministry of Emergency Management, International Federation of Red Cross and Red Crescent Societies

Government of Kerala (2018a) Memorandum (Revised): Monsoon calamity losses 29th May to 31st July 2018a. Available at https://sdma.kerala.gov.in/disaster-memoranda/

Government of Kerala (2018b) Kerala floods - 2018b: 1st August to 30th August 2018b. Available at https://sdma.kerala.gov.in/disaster-memoranda/

Government of Kerala (2019a) Memorandum: Kerala floods – 2019a (1st August to 31st August 2019a). Available at https://sdma.kerala.gov.in/disaster-memoranda/

Government of Kerala (2019b) Rebuild kerala development programme. Rebuild Kerala Initiative, Government of Kerala. Available at https://rebuild.kerala.gov.in/en/rebuild

Grimnes S, Martinsen ØG (2015) Data and models. Bioimpedance and bioelectricity basics. Elsevier, pp 329–404. https://doi.org/10.1016/B978-0-12-411470-8.00009-X

Hajat S, Ebi KL, Kovats RS, Menne B, Edwards S, Haines A (2005) The human health consequences of flooding in Europe: a review. In: Kirch W, Bertollini R, Menne B (eds) Extreme Weather Events and Public Health Responses. Springer-Verlag, Berlin/Heidelberg, pp 185–196. https://doi.org/10.1007/3-540-28862-7_18

Hanley JA, McNeil BJ (1982) The meaning and use of the area under a receiver operating characteristic (ROC) curve. Radiology 143:29–36

Hao L, Rajaneesh A, van Westen C, Sajinkumar KS, Martha TR, Jaiswal P, McAdoo BG (2020) Constructing a complete landslide inventory dataset for the 2018 Monsoon disaster in Kerala, India, for land use change analysis. Earth Syst Sci Data 12(4):2899–2918. https://doi.org/10.5194/essd-12-2899-2020

Hao L, Cees van Westen A, Rajaneesh KSS, Martha TR, Jaiswal P (2022) Evaluating the relation between land use changes and the 2018 landslide disaster in Kerala, India. CATENA 216:106363. https://doi.org/10.1016/j.catena.2022.106363

Hoffmann R, Blecha D (2020) Education and disaster vulnerability in Southeast Asia: evidence and policy implications. Sustainability 12(4):1401. https://doi.org/10.3390/su12041401

Hoque MAA, Tasfia S, Ahmed N, Pradhan B (2019) Assessing spatial flood vulnerability at Kalapara Upazila in Bangladesh using an analytic hierarchy process. Sensors 19(6):1302. https://doi.org/10.3390/s19061302

Hosmer DW, Lemeshow S (2000) Applied logistic regression, 2nd Ed. Chapter 5, John Wiley and Sons, New York, NY, pp 160–164

Hunt KMR, Menon A (2020) The 2018 Kerala floods: a climate change perspective. Clim Dyn 54:2433–2446. https://doi.org/10.1007/s00382-020-05123-7

Hussain M, Tayyab M, Zhang J, Shah AA, Ullah K, Mehmood U, Al-Shaibah B (2021) GIS-based multi-criteria approach for flood vulnerability assessment and mapping in district Shangla: Khyber Pakhtunkhwa, Pakistan. Sustainability 13(6):3126. https://doi.org/10.3390/su13063126

Joshi A, Dhumka A, Dhiman Y, Rawat C, Ritika (2022) A comparative study of supervised learning techniques for remote sensing image classification. In: Sharma TK, Ahn CW, Verma OP, Panigrahi BK (eds) Soft computing: theories and applications: proceedings of SoCTA 2020, Volume 1. Springer Singapore, Singapore, pp 49–61. https://doi.org/10.1007/978-981-16-1740-9_6

Khashei-Siuki A, Keshavarz A, Sharifan H (2020) Comparison of AHP and FAHP methods in determining suitable areas for drinking water harvesting in Birjand aquifer. Iran Groundw Sustain Dev. https://doi.org/10.1016/j.gsd.2019.100328

Lee JY, Kim JS (2021) Detecting areas vulnerable to flooding using hydrological-topographic factors and logistic regression. Appl Sci. https://doi.org/10.3390/app11125652

Liu Y, Eckert CM, Earl C (2020) A review of fuzzy AHP methods for decision-making with subjective judgements. Expert Syst Appl. https://doi.org/10.1016/j.eswa.2020.113738

Liu T, Shi P, Fang J (2022) Spatiotemporal variation in global floods with different affected areas and the contribution of influencing factors to flood-induced mortality (1985–2019). Nat Hazards. https://doi.org/10.1007/s11069-021-05150-5

Mishra V, Shah HL (2018) Hydroclimatological perspective of the Kerala flood of 2018. J Geol Soc India 92:645–650. https://doi.org/10.1007/s12594-018-1079-3

Nicholls R, Zanuttigh B, Vanderlinden JP, Weisse R, Silva R, Hanson S, Narayan S, Hoggart S, Thompson RC, de Vries W, Koundouri P (2015) Developing a holistic approach to assessing and managing coastal flood risk. Coastal risk management in a changing climate. Elsevier, pp 9–53. https://doi.org/10.1016/B978-0-12-397310-8.00002-6

Nikhil S, Danumah JH, Saha S, Prasad MK, Rajaneesh A, Mammen PC, Ajin RS, Kuriakose SL (2021) Application of GIS and AHP method in forest fire risk zone mapping: a study of the Parambikulam Tiger Reserve, Kerala, India. J Geovisualiz Spatial Anal. https://doi.org/10.1007/s41651-021-00082-x

Ochoa C, Bolon I, Durso AM, de Castañeda RR, Alcoba G, Martins SB, Chappuis F, Ray N (2020) Assessing the increase of snakebite incidence in relationship to flooding events. J Environ Public Health. https://doi.org/10.1155/2020/6135149

Okaka FO, Odhiambo BDO (2018) Relationship between flooding and out break of infectious diseases in Kenya: a review of the

literature. J Environ Public Health. https://doi.org/10.1155/2018/5452938
Olson DL (1988) Opportunities and limitations of AHP in multiobjective programming. Math Comput Model 11:206–209. https://doi.org/10.1016/0895-7177(88)90481-5
Paranjothy S, Gallacher J, Amlôt R, Rubin GJ, Page L, Baxter T, Wight J, Kirrage D, McNaught R, Palmer SR (2011) Psychosocial impact of the summer 2007 floods in England. BMC Public Health. https://doi.org/10.1186/1471-2458-11-145
Peek L (2008) Children and disasters: understanding vulnerability, developing capacities, and promoting resilience: an introduction. Child Youth Environ 18(1):1–29. https://doi.org/10.7721/chilyoutenvi.18.1.0001
Pradeep GS, Danumah JH, Nikhil S, Prasad MK, Patel N, Mammen PC, Rajaneesh A, Oniga VE, Ajin RS, Kuriakose SL (2022) Forest fire risk zone mapping of Eravikulam national park in India: a comparison between frequency ratio and analytic hierarchy process methods. Croatian J For Eng 43(1):199–217. https://doi.org/10.5552/crojfe.2022.1137
Putra MSD, Andryana S, Fauziah GA (2018) Fuzzy analytical hierarchy process method to determine the quality of gemstones. Adv Fuzzy Syst. https://doi.org/10.1155/2018/9094380
Qazi WA, Abushammala MFM (2020) Multi-criteria decision analysis of waste-to-energy technologies. waste-to-energy. Elsevier, pp 265–316. https://doi.org/10.1016/B978-0-12-816394-8.00010-0
Radmehr A, Araghinejad S (2015) Flood vulnerability analysis by fuzzy spatial multi criteria decision making. Water Resour Manag 29:4427–4445. https://doi.org/10.1007/s11269-015-1068-x
Rahman M, Ningsheng C, Islam MM, Dewan A, Iqbal J, Washakh RMA, Shufeng T (2019) Flood susceptibility assessment in Bangladesh using machine learning and multi-criteria decision analysis. Earth Syst Environ 3:585–601. https://doi.org/10.1007/s41748-019-00123-y
Rasch RJ (2016) Assessing urban vulnerability to flood hazard in Brazilian municipalities. Environ Urban 28(1):145–168. https://doi.org/10.1177/0956247815620961
Rouse JW, Haas RH, Schell JA, Deering DW (1974) Monitoring vegetation systems in the Great Plains with ERTS. In: Freden SC, Mercanti EP, Becker MA (eds) Proceedings of the Third Earth Resources Technology Satellite-1 Symposium. NASA, Washington D.C., USA, pp. 309–317
Saaty TL (1980) The analytic hierarchy process: planning, priority setting, resource allocation (Decision making series). McGraw Hill, New York
Saha S, Sarkar D, Mondal P (2021) Efficiency exploration of frequency ratio, entropy and weights of evidence-information value models in flood vulnerability assessment: a study of Raiganj subdivision. Stochastic Environ Res Risk Assess Eastern India. https://doi.org/10.1007/s00477-021-02115-9
Sajinkumar KS, Arya A, Rajaneesh A, Oommen T, Yunus Ali P, Rani VR, Thrivikramji KP (2022) Migrating rivers, consequent paleochannels: the unlikely partners and hotspots of flooding. Sci Total Environ 807:150842. https://doi.org/10.1016/j.scitotenv.2021.150842
Samanta S, Pal DK, Palsamanta B (2018) Flood susceptibility analysis through remote sensing, GIS and frequency ratio model. Appl Water Sci. https://doi.org/10.1007/s13201-018-0710-1
Sam AS, Kumar R, Kächele H, Müller K (2017) Vulnerabilities to flood hazards among rural households in India. Nat Hazards 88:1133–1153. https://doi.org/10.1007/s11069-017-2911-6
Sarkar D, Mondal P (2020) Flood vulnerability mapping using frequency ratio (FR) model: a case study on Kulik river basin. Indo-Bangladesh Barind Region Applied Water Sci. https://doi.org/10.1007/s13201-019-1102-x
Seyedin H, HabibiSaravi R, Sayfouri N, Djenab VH, Hamedani FG (2017) Psychological sequels of flood on residents of southeast Caspian region. Nat Hazards 88:965–975. https://doi.org/10.1007/s11069-017-2926-z
Shahfahad MM, Kumari B, Tayyab M, Paarcha A, Asif RA (2021) Indices based assessment of built-up density and urban expansion of fast growing Surat city using multi-temporal Landsat data sets. GeoJournal 86:1607–1623. https://doi.org/10.1007/s10708-020-10148-w
Shen L, Li C (2010) Water body extraction from Landsat ETM$^+$ imagery using adaboost algorithm. In: Proceedings of 18th International Conference on Geoinformatics. Beijing, China, pp 1–4. https://doi.org/10.1109/GEOINFORMATICS.2010.5567762
Sisodia PS, Tiwari V, Kumar A (2014) Analysis of supervised maximum likelihood classification for remote sensing image. In: Proceedings of the International Conference on Recent Advances and Innovations in Engineering (ICRAIE-2014), pp. 1–4. https://doi.org/10.1109/ICRAIE.2014.6909319
Smith K, Ward R (1998) Floods: Physical process and human impacts. Wiley, Chichester
Sunar Erbek F, Özkan C, Taberner M (2004) Comparison of maximum likelihood classification method with supervised artificial neural network algorithms for land use activities. Int J Remote Sens 25(9):1733–1748. https://doi.org/10.1080/0143116031000150077
Sun R, An D, Wei L, Shi Y, Wang L, Zhang C, Zhang P, Qi H, Wang Q (2016) Impacts of a flash flood on drinking water quality: case study of areas most affected by the 2012 Beijing flood. Heliyon 2(2):e00071. https://doi.org/10.1016/j.heliyon.2016.e00071
Swain DL, Wing OEJ, Bates PD, Done JM, Johnson KA, Cameron DR (2020a) Increased flood exposure due to climate change and population growth in the United States. Earth's Future. https://doi.org/10.1029/2020EF001778
Swain KC, Singha C, Nayak L (2020) Flood susceptibility mapping through the GIS-AHP technique using the cloud. ISPRS Int J Geo-Inf 9(12):720. https://doi.org/10.3390/ijgi9120720
Tabari H (2020) Climate change impact on flood and extreme precipitation increases with water availability. Sci Rep. https://doi.org/10.1038/s41598-020-70816-2
Tascón-González L, Ferrer-Julià M, Ruiz M, García-Meléndez E (2020) Social vulnerability assessment for flood risk analysis. Water 12(2):558. https://doi.org/10.3390/w12020558
Tehrany MS, Pradhan B, Mansor S, Ahmad N (2015) Flood susceptibility assessment using GIS-based support vector machine model with different kernel types. CATENA 125:91–101. https://doi.org/10.1016/j.catena.2014.10.017
Thomas AV, Saha S, Danumah JH, Raveendran S, Prasad MK, Ajin RS, Kuriakose SL (2021) Landslide susceptibility zonation of Idukki district using GIS in the aftermath of 2018 Kerala floods and landslides: A comparison of AHP and frequency ratio methods. J Geovisualiz Spatial Anal. https://doi.org/10.1007/s41651-021-00090-x
Thompson JA, Roecker S, Grunwald S, Owens PR (2012) Digital soil mapping. hydropedology. Elsevier, pp 665–709. https://doi.org/10.1016/B978-0-12-386941-8.00021-6
Tripathi AK, Agrawal S, Gupta RD (2021) Comparison of GIS-based AHP and fuzzy AHP methods for hospital site selection: a case study for Prayagraj City. GeoJournal, Prayagraj. https://doi.org/10.1007/s10708-021-10445-y
UNDP (2018) Kerala post disaster needs assessment: floods and landslides - August 2018. Available at https://www.undp.org/publications/post-disaster-needs-assessment-kerala
Vanama VSK, Rao YS, Bhatt CM (2021) Change detection based flood mapping using multi-temporal earth observation satellite

images: 2018 flood event of Kerala. India Eur J Remote Sens 54(1):42–58. https://doi.org/10.1080/22797254.2020.1867901

Viana CM, Oliveira S, Oliveira SC, Rocha J (2019) Land use/land cover change detection and urban sprawl analysis. Spatial modeling in GIS and R for earth and environmental sciences. Elsevier, pp 621–651. https://doi.org/10.1016/B978-0-12-815226-3.00029-6

Vishnu CL, Sajinkumar KS, Oommen T, Coffman RA, Thrivikramji KP, Rani VR, Keerthy S (2019) Satellite-based assessment of the August 2018 Flood in parts of Kerala, India. Geomat Nat Haz Risk 10(1):758–767. https://doi.org/10.1080/19475705.2018.1543212

Vishnu CL, Rani VR, Sajinkumar KS, Oommen T, Bonali FL, Pareeth S, Thrivikramji K, McAdoo BG, Anilkumar Y, Rajaneesh A (2020) Catastrophic flood of August 2018, Kerala, India: partitioning role of geologic factors in modulating flood level using remote sensing data. Remote Sens Appl Soc Environ. https://doi.org/10.1016/j.rsase.2020.100426

Winter MG, Shearer B, Palmer D, Peeling D, Harmer C, Sharpe J (2016) The economic impact of landslides and floods on the road network. Procedia Eng 143:1425–1434. https://doi.org/10.1016/j.proeng.2016.06.168

Wubalem A (2021) Landslide susceptibility mapping using statistical methods in Uatzau catchment area, northwestern Ethiopia. Geoenviron Dis. https://doi.org/10.1186/s40677-020-00170-y

Xu H (2006) Modification of normalised difference water index (NDWI) to enhance open water features in remotely sensed imagery. Int J Remote Sens 27(14):3025–3033. https://doi.org/10.1080/01431160600589179

Yard EE, Murphy MW, Schneeberger C, Narayanan J, Hoo E, Freiman A, Lewis LS, Hill VR (2014) Microbial and chemical contamination during and after flooding in the Ohio River: Kentucky, 2011. J Environ Sci Health Part A 49(11):1236–1243. https://doi.org/10.1080/10934529.2014.910036

Yun D, Zhang Y, Ling F, Wang Q, Li W, Li X (2016) Water bodies' mapping from Sentinel-2 imagery with modified normalized difference water index at 10-m spatial resolution produced by sharpening the SWIR band. Remote Sens 8(4):354. https://doi.org/10.3390/rs8040354

Yurdagül Kumcu S (2022) Flood management under changing climate. In: Bahadir M, Haarstrick A (eds) Water and wastewater management: global problems and measures. Springer International Publishing, Cham, pp 35–40. https://doi.org/10.1007/978-3-030-95288-4_4

Zha Y, Gao J, Ni S (2003) Use of normalized difference built-up index in automatically mapping urban areas from TM imagery. Int J Remote Sens 24(3):583–594. https://doi.org/10.1080/01431160304987